1 **Title:** Perturbation increases source-dependent organic matter degradation rates in estuarine

2 sediments.

3

4 **Author information**

5 Guangnan Wu[1], Klaas G.J. Nierop[2], Bingjie Yang[3], Stefan Schouten[3], Gert-Jan Reichart[1, 2], Peter

6 Kraal[1]

7

8 [1] Royal Netherlands Institute for Sea Research, Department of Ocean Systems, Landsdiep 4, 1797

9 SZ 't Horntje, The Netherlands

10 [2] Utrecht University, Faculty of Geosciences, Princetonlaan 8a, 3584 CB Utrecht, The Netherlands

11 [3] Royal Netherlands Institute for Sea Research, Department of Marine Microbiology &

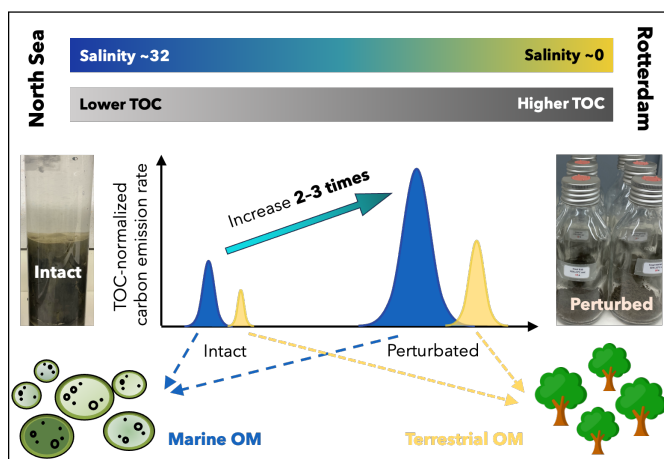12 Biogeochemistry, Landsdiep 4, 1797 SZ 't Horntje, The Netherlands

13

14 **Corresponding author**

15 Guangnan Wu (guangnan.wu@nioz.nl)

16

17

Abstract

Despite a relatively small surface area on Earth, estuaries play a disproportionally important role in the global carbon cycle due to their relatively high primary production and rapid organic carbon processing. Estuarine sediments are highly efficient in preserving organic carbon and thus often rich in organic matter (OM), highlighting them as important reservoirs of global blue carbon. Currently, estuaries are facing intensified human disturbance, one of which is sediment dredging. To understand estuarine carbon dynamics and the impact of perturbations, insights into sediment OM sources, composition, and degradability are required. We characterized the sediment OM properties and oxidation rates in one of the world's largest ports, the Port of Rotterdam, located in a major European estuary. Using a combination of OM source proxies and end-member modeling analysis, we quantified the contributions of marine (10–65%), riverine (10–60%), and terrestrial (10–65%) OM inputs across the investigated transect, with salinity ranging from 32 (marine) to almost 0 (riverine). Incubating intact sediment cores from two contrasting sites (marine versus riverine) suggested that OM degradation rates in marine sediments were about four times higher than those in riverine sediments, which was also observed during a 35-day subaerial bottle incubation experiment with mixed surface sediment. Moreover, subaerial incubation of mixed sediment showed a two- to three-fold increase in OM degradation rates compared to intact core incubation, highlighting that perturbation and subsequent enhanced oxygen availability can substantially boost OM degradation. By combining detailed quantitative characterization of estuarine OM properties with degradation experiments under varying conditions, the results further our understanding of the factors that govern OM degradation rates in (perturbed) estuarine systems. Ultimately, this contributes to constraining the impact of human perturbation on OM cycling in estuaries and its role in the carbon cycle.

Graphical abstract

1. Introduction

Estuaries are highly dynamic aquatic systems that are influenced by simultaneous marine, riverine, and terrestrial inputs. In this transition zone, strong and variable gradients exist in hydrodynamic and sediment properties, resulting in dynamic and complex cycles of key elements such as carbon through coupled physical, chemical, and biological processes (Barbier et al., 2011; Dürr et al., 2011; Laruelle et al., 2010). Despite representing only 0.03% of the surface area of marine systems, estuaries are estimated to release approximately 0.25 Pg carbon annually into atmosphere on a global scale, which is equivalent to 17% of the air-water CO_2 gas exchange of the entire open ocean (Bauer et al., 2013; Li et al., 2023). Additionally, estuarine sediments store large amounts of organic carbon (Macreadie et al., 2019; McLeod et al., 2011); due to high productivity and high sedimentation rates, carbon burial rates in estuaries are up to one order of magnitude higher than forest soils and three orders of magnitude higher than in open ocean sediments (Kuwae et al., 2016). Their disproportionally large importance in the global carbon cycle highlights the need to improve our understanding of carbon dynamics in estuarine systems.

Organic matter (OM), a fundamental component of sediment, plays a key role in sediment carbon fluxes and sequestration. Degradation of OM contributes to the release of carbon dioxide (CO_2) and methane (CH_4). This is a dynamic process that proceeds through a series of enzymatic reactions involving different organisms, oxidants, and intermediate compounds. Studies have pointed out the importance of OM characteristics in influencing the rate and extent of OM degradation (Burd et al., 2016; Burdige, 2007; LaRowe and Van Cappellen, 2011). For instance, extensively degraded OM and biopolymers such as cellulose and lignin are less susceptible to degradation than freshly produced nitrogenous compounds (Arndt et al., 2013). Estuarine systems have diverse terrestrial and aquatic OM sources, exhibiting varying degrees of degradability (Canuel and Hardison, 2016). Moreover, interactions between OM and other components (organic or inorganic) during transportation, deposition, and mineralization can alter OM characteristics. Processes such as condensation, (geo)polymerization and mineral association increase OM resistance to degradation, thereby promoting OM preservation (Wakeham and Canuel, 2006).

Sediment OM degradation is also influenced by ambient conditions at the sediment-water interface and in the sediment (Arndt et al., 2013; Burd et al., 2016; Burdige, 2007; LaRowe and Van Cappellen, 2011). The degradation pathway follows the sequential utilization of the terminal electron acceptors (TEAs), typically in the order of O_2, NO_3^-/NO_2^-, Mn (IV), Fe (III) and SO_4^{2-}, with a progressive decrease in energy yield down the redox ladder. The availability of these TEAs is greatly influenced by the depositional environment. Estuaries are highly dynamic systems with strong and shifting salinity (i.e. sulfate) gradients exist. This results in strong spatial variability in OM degradation pathways and carbon dynamics (Cao et al., 2021). Specifically, large fluctuations in salinity and thus sulfate (SO_4^{2-}) availability between sites will affect CH_4 emissions because sulfate-driven methane oxidation provides a highly effective CH_4 filter in surface sediments (e.g. Egger et al., 2018; Lovley and Phillips, 1986). Moreover, compilation of field data reveals that organic carbon burial efficiency varies substantially in

85   space because the availability and exposure time of TEAs are influenced by environmental factors
86   such as sedimentation rate (Arndt et al., 2013; Freitas et al., 2021). Estuaries are often characterized
87   by relatively high sedimentation rates, with supply of riverine material that settles under low flow
88   velocities at the river mouths as well as large inputs of (re)suspended marine matter from the coastal
89   zone (Hutchings et al., 2020) . Oxygen transport into the sediment is sufficiently low relative to the flux
90   of reactive organic carbon to these sediments to maintain very shallow oxygen penetration depths, on
91   the scale of micro- to millimeters (Burdige, 2012). By notably reintroducing O_2 to OM previously buried
92   in oxygen-limited environments, sediment disturbance caused by natural processes (e.g. storm-
93   induced mixing events, bioturbation) and human activities (e.g. dredging, bottom trawling) can change
94   sediment redox chemistry and thereby have a profound effect on OM degradation pathways and
95   burial efficiency (Aller, 1994).
96
97   Although estuaries have been widely studied from an ecological perspective, large variation in OM
98   properties and cycling processes within and across estuarine systems contributes to the uncertainty in
99   quantifying their significance in the global carbon cycle. This uncertainty is partially due to the highly
100   diverse OM sources and properties in estuarine systems. Many studies of estuarine OM sources use
101   bulk proxies such as the weight ratio of total organic carbon to total nitrogen (C/N ratio) and their
102   stable isotope ratios ($\delta^{13}C_{org}$ and $\delta^{15}N$; Canuel and Hardison, 2016; Carneiro et al., 2021; Cloern et
103   al., 2002; Middelburg and Nieuwenhuize, 1998). In other studies, OM sources have been investigated
104   by identifying biomarker compounds associated with specific sources and transformation processes.
105   For example, the branched and isoprenoid tetraether (BIT) index, based on the relative abundance of
106   terrestrially and/or freshwater-derived branched glycerol dialkyl glycerol tetraether (GDGT) versus
107   marine-derived isoprenoid GDGT crenarchaeol, was adopted to quantify the relative contribution of
108   terrestrial OM in sediments (Herfort et al., 2006; Hopmans et al., 2004; Smith et al., 2010; Strong et
109   al., 2012). Some studies focused on macromolecular organic matter (MOM) composition in sediments
110   to identify OM sources (Kaal et al., 2020; Nierop et al., 2017). Lignin, an important constituent of
111   vascular plant MOM, has proved to be a useful tracer of vascular plant inputs to estuarine/coastal
112   margin sediment (Bianchi and Bauer, 2012; Buurman et al., 2006; Fabbri et al., 2005; Hedges and
113   Oades, 1997; Kaal, 2019). Furthermore, the relationship between OM source and degradability can
114   be intricate, which inhibits the quantitative understanding of estuarine OM degradation.
115
116   Understanding the processing of OM within estuaries takes on further importance because many
117   estuarine systems are intensively altered by human activities (Arndt et al., 2013; Heckbert et al.,
118   2012; Holligan and Reiners, 1992). To increase or maintain waterway navigability, dredging is
119   commonly practiced in many coastal regions and rivers worldwide. More than 600 million m^3 of
120   dredged material is generated annually just in Western Europe, China, and the USA (Amar et al.,
121   2021). While the dredged sediments are often treated as waste and disposed of at sea, there is a
122   growing trend of reusing dredged sediments on land, for instance in beach nourishment, habitat
123   restoration, and land reclamation (Brils et al., 2014). However, this impacts organic matter
124   degradation and subsequent CO_2 release from dredged materials in currently poorly understood

ways, with oxygen exposure potentially leading to enhanced carbon remineralization (LaRowe et al., 2020). Given the need for sediment dredging and sustainable management of these materials (van de Velde et al., 2018), it is of great importance to understand to what extent anthropogenic sediment perturbations affect OM processing in and carbon emissions from estuarine sediments.

In this study, we investigate the spatial variability in OM content and properties and relationships between OM source, composition, and degradability along a salinity gradient in the profoundly disturbed Port of Rotterdam estuarine environment of the Rhine-Meuse delta system. Given the frequent dredging activities in the study area, which hosts a globally major port, we aim to understand the impact of sediment dredging and its potential land applications on carbon dynamics. We used a combination of bulk OM proxies, BIT index, macromolecular organic matter (MOM) composition analysis, as well as end-member modelling to understand OM sources and composition. Furthermore, organic matter degradation rates were estimated both in 8-h sediment core incubation (mimicking in situ condition) and 37-day bottle incubations with mixed surface sediments under atmospheric conditions (representing subaerial application of dredged sediment). This study shows that variability in OM sources and subsequently molecular properties, as well as perturbation (i.e. introduction of oxygen), have important effects on OM degradation rates, providing important implications for estuarine sediment management strategies.

2. Materials and methods

2.1. Study area and sample collection

The study area is located in the northern part of the Rhine-Meuse estuary (Fig. 1), spanning from Rotterdam city to the Maasmond. This area representing a transitional environment from riverine to marine is heavily urbanized and hosts one of the world's largest ports, the Port of Rotterdam (PoR). Every year, large amounts of sediment are deposited in the harbor from both rivers as well as the North Sea (Kirichek et al., 2018). The water channel maintenance and harbor expansion lead to an increasing need for sediment dredging throughout the PoR. Due to higher sedimentation rates and the demand for deeper navigation channels at the river mouth, dredging is more frequently performed in the western (marine) part (e.g. site 115) than in the eastern (riverine) part (e.g. 21A; Kirichek et al., 2018). Currently, over 10 million m^3 of dredged materials are generated from the PoR annually, most sediments (classified as clean) being relocated to the shallow North Sea, while approximately 10% (classified as contaminated) being stored subaerially in a holding basin in the PoR area (Kirichek et al., 2018).

Bulk sediments were collected from 49 selected locations throughout the study area in the summer of 2021. These sites were selected from over 300 monitoring sites in the Port of Rotterdam to represent the full spectrum of depositional conditions in the main waterway and adjacent harbor areas from marine to riverine (Fig. 1). One sediment core from each site was collected using a gravity corer (⌀9 cm). Once on deck, materials in the corer (down to ~50 cm depth) were emptied into 5-L polypropylene buckets that were closed and stored in the fridge at 4 °C. These samples, later referred

165 as bulk sediments, were further processed within a week after collection at the Royal Netherlands
166 Institute for Sea Research (NIOZ) on Texel, the Netherlands. In addition to bulk sediments, intact
167 sediment cores were collected in summer 2022 upon revisiting two strongly contrasting sites (referred
168 as 'super sites' in Fig. 1) representing marine (site 115, salinity 29) and riverine (site 21A, salinity 5)
169 end-members in the PoR area. The intact sediment cores were immediately cooled, transported back
170 to the NIOZ and used in whole-core incubation experiments (see section 2.5) within 5 hours after
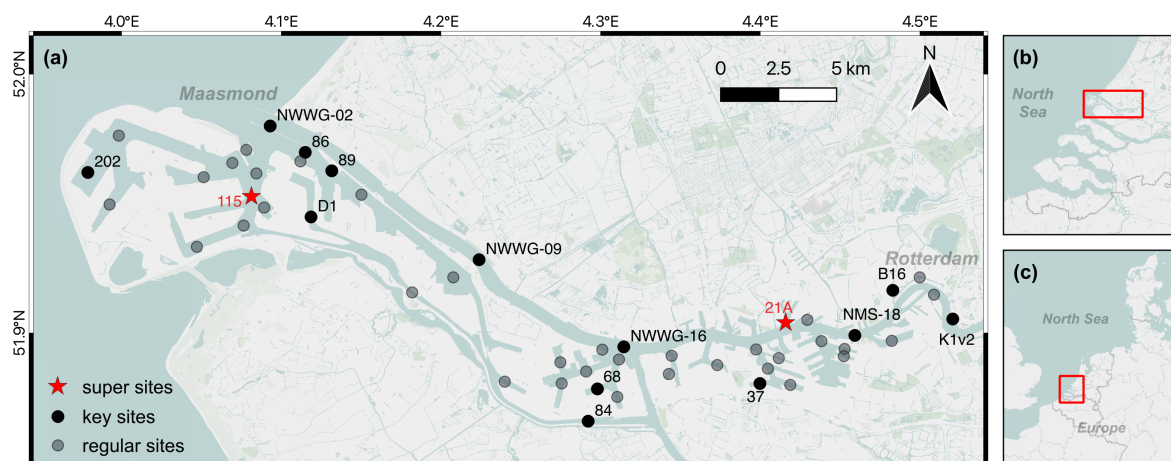171 collection.

173
174 **Fig. 1.** (a) The investigated study area and sampling sites. Sediments from all 49 sites were subjected
175 to bulk analyses (e.g. grain size, TOC, TN) as detailed in section 2.2. Sediments from 13 key sites
176 were used for lipid and MOM analysis as detailed in section 2.3 and 2.4, respectively. Sediment cores
177 from two super sites were used in a whole-core incubation experiment as detailed in section 2.5. (b)
178 The location of investigated study area in the Rhine–Meuse estuary. (c) The location of Rhine-Meuse
179 estuary in Western Europe. Map created using QGIS software. Basemap courtesy of Mapbox.

180
181 **2.2. Sample processing and analysis**
182 Bulk sediments from each of the 49 sites were thoroughly mixed using a spatula in the buckets.
183 Approximately 40 mL of wet sediment were transferred into 50-mL polypropylene centrifuge tubes
184 (Falcon) and centrifuged at 3000 rpm for 20 min (Hermle Z 446). In a N_2-purged glove bag, the
185 porewater was immediately filtered through a 0.45-µm nylon syringe filter (MDI). Salinity was
186 estimated by comparing the porewater sodium (Na) concentration to the average seawater sodium
187 concentration and salinity in the North Sea (IJsseldijk et al., 2015; Steele et al., 2010). For Na
188 analysis, the porewater was diluted around 900 times in 1 M double-distilled HNO_3 and analyzed by
189 inductively coupled plasma mass spectrometry (ICP-MS, Thermo Scientific, Element 2).

190
191 The centrifuge tubes with wet sediment residues after centrifugation were purged with N_2 and stored
192 at −20 ºC in N_2-purged, gas-tight Al-laminate bags to prevent oxidation. To prepare for subsampling,
193 the sediment residues were thawed overnight in a N_2-purged glove bag (Coy Laboratories) and
194 subsequently homogenized. One portion of wet sediment residue (~1 g) was mixed with 50 mL of 3 g

195 L^{-1} sodium pyrophosphate solution and gently shaken to disaggregate particles. Particle size

196 distribution was determined using a Coulter laser particle sizer (Beckman Coulter), from which

197 percentages of clay (0–2 μm), silt (2–63 μm), sand (63–2000 μm) and the median particle size (D50)

198 were calculated.

199

200 Approximately 10 g of wet sediment residue was freeze-dried (Hetosicc freeze dryer) for 72 h and

201 manually ground with an agate pestle and mortar, and further subsampled for carbon and nitrogen

202 (CN) analysis. One subsample of the freeze-dried sediment (~10 mg) was directly used for measuring

203 total nitrogen (TN) and stable nitrogen isotope composition (expressed as δ^{15}N, relative to

204 atmospheric nitrogen) by a CN elementary analyzer (Thermo Scientific, FLASH 2000) coupled to a

205 Delta V Advantage isotope ratio mass spectrometer (Thermo Scientific). Another freeze-dried

206 subsample (~0.5 g), firstly treated with 1 M HCl to remove carbonates, was used for measuring total

207 organic carbon (TOC) and stable carbon isotope composition (expressed as δ^{13}C$_{org}$, relative to Vienna

208 Pee Dee Belemnite). Certified laboratory standards (acetanilide, urea, and casein) were used for

209 calibration with each sample. Precision and accuracy for standards and triplicate samples were

210 ±0.3‰ for δ^{13}C$_{org}$ and δ^{15}N, and the relative standard deviation (RSD; standard deviation/mean) was

211 <10% for TOC and TN.

212

213 **2.3. Lipid extraction and analysis**

214 Sediments from 13 key locations (Fig. 1), selected to cover the full river-marine salinity transect, were

215 used for lipid and MOM analyses. Freeze-dried and homogenized sediments (2–10 g) were

216 ultrasonically extracted with dichloromethane (DCM):methanol (2:1, v:v) five times. For each sample,

217 extracts obtained from the five steps were combined. The total extract was separated over an Al$_2$O$_3$

218 column into an apolar, neutral and polar fraction using hexane:DCM (9:1, v:v), hexane:DCM (1:1, v:v)

219 and DCM:methanol (1:1, v:v), respectively. The polar fractions containing glycerol dialkyl glycerol

220 tetraethers (GDGTs) were dried under N$_2$, dissolved in hexane:propanol (99:1, v:v), and filtered using

221 a 0.45 μm PTFE filter. This fraction was subsequently analyzed with ultra-high performance liquid

222 chromatography mass spectrometry (UHPLC-MS) on an Agilent 1260 Infinity HPLC coupled to an

223 Agilent 613MSD according to (Hopmans et al., 2016). The isoprenoid and branched GDGTs were

224 detected by scanning for their [M+H]$^+$ ions. The BIT index was calculated according to (Hopmans et

225 al., 2004).

226

227 **2.4. Macromolecular organic matter (MOM) isolation and analysis**

228 The sediment residues, remaining after lipid extraction, from the 13 samples from key locations were

229 dried under N$_2$. To isolate MOM, dried sediment residue (2–3 g) was transferred into 50-mL centrifuge

230 tubes and decalcified with 30 mL 1 M HCl for 4 h, later rinsed twice with 25 mL milli-Q water (18 MΩ).

231 After centrifugation and decanting the supernatant, 15-mL 40% HF (analytical grade, Merck) was

232 added and shaken for 2 h at 100 rpm. The solution was diluted with milli-Q water to 50 mL and left

233 standing overnight, after which the solution was decanted to a high-density polyethylene plastic

234 container designated for HF waste. A volume of 15 mL 30% HCl was added and subsequently diluted

235 with milli-Q water to 50 mL. After shaking for 1 h and centrifugation, the solution was decanted, and

236 the residues were washed with milli-Q water three times to neutralize pH and subsequently freeze-

237 dried. The supernatant of all steps was collected in the HF waste container. Samples were

238 desulfurized using activated copper pellets in DCM. Suspensions were stirred overnight after which

239 the copper pellets and DCM were removed. The sample residue, containing the macromolecular

240 organic matter (MOM), was air-dried prior to the analysis.

241

242 The analysis of MOM was conducted at Utrecht University using the pyrolysis-gas chromatograph-

243 mass spectrometry method previously described in (Nierop et al., 2017). In short, the isolated MOM

244 was pyrolyzed on a Horizon Instruments Curie-Point pyrolysis unit. The pyrolysis unit was connected

245 to a Carlo Erba GC8060 gas chromatograph and the products were separated by a fused silica

246 column (CP-Sil5, 25 m, 0.32 mm i.d.) coated with CP-Sil5 (film thickness 0.40 μm). The column was

247 coupled to a Fisons MD800 mass spectrometer. Pyrolysis products were identified using a NIST

248 library or by interpretation of the spectra, by their retention times and/or by comparison with literature

249 data. Quantification was performed according to (Nierop et al., 2017).

250

251 **2.5. Whole-core sediment incubation**

252 Triplicate intact sediment cores collected from two strongly contrasting sites (marine site 115 vs.

253 riverine site 21A) were used for whole-core incubation. These sites represent relatively intensively

254 dredged marine and riverine areas, respectively, that contribute significantly to the total annual

255 dredged sediment volume in the PoR. Prior to incubation, cores were carefully manipulated to have

256 ~15 cm of undisturbed top sediment (primary zone of diagenesis) with ~20 cm of overlying water

257 (achieving a ~ 1:1 water:sediment volume ratio which represents a balance between sensitivity in

258 measuring fluxes while avoiding excess accumulation of (inhibiting) reactants in the overlying water

259 and ensuring a small fraction of the overlying water is replaced by discrete sampling). After confirming

260 that the sediment surface was not disturbed, an oxygen sensor spot (Presens) was attached to the

261 inner wall of the core tube (5 cm from the top) to monitor O_2 in the overlying water. The cores, capped

262 at the bottom and open at the top, were submerged in bottom water from the corresponding site in an

263 incubation tank. Stirrers were placed in each core to mix the overlying water (at ~1 rpm) and the cores

264 were left open overnight to equilibrate. The water in the tank was kept fully oxygenated by sparging

265 with air using an aquarium pump. Temperature in the room was maintained at the measured in situ

266 bottom water temperature (19 °C). At the start of the incubation, the cores were capped with gas-tight

267 lids with an outlet to sample bottom water from the core and an inlet to replace sampled volume with

268 site water from a 20-L reservoir. Over the course of an eight-hour incubation period, 30 mL of bottom

269 water (equivalent to 2.3% of total overlaying water volume) were extracted at pre-determined time

270 intervals of 0, 1.5, 3.5, 5, 6.5, and 8 h. The dissolved O_2 concentration in the overlying water in each

271 core was measured every five minutes using the sensor spots and a Presens OXY-4 SMA meter with

272 fiber optic cables, operated using Presens Measurement Studio 2. Immediately after sampling, the

273 water samples were filtered using 0.45-μm nylon syringe filters for dissolved inorganic carbon (DIC),

total alkalinity (TA) and dissolved inorganic nitrogen (DIN: NH_4^+, NO_3^-, NO_2^-) analysis, while an unfiltered subsample was retained for methane (CH_4) analysis.

The DIC samples were diluted 10 times in N_2-purged 25 g L^{-1} sodium chloride solution without headspace and analyzed within 24 hours on a continuous flow analyzer (QuAAtro, Seal Analytical). The TA samples were kept at 5 °C without treatment and measured within a week using the same analyzer. The DIN samples were stored at −20 °C and later analyzed on a TRAACS 800+ continuous flow analyzer. For CH_4, 12 mL of bottom water was directly transferred into a 12 mL Exetainer vial (Labco), immediately poisoned with ~0.25 mL of saturated zinc chloride solution and capped with a butyl rubber stopper ensuring no headspace was present. Dissolved CH_4 concentration was determined using a headspace technique (Magen et al., 2014). Prior to the measurement, 1 mL of N_2 headspace was injected through the stopper in each Exetainer vial while a needle allowed the equivalent volume of sample to escape, after which the samples were equilibrated for a week. Headspace CH_4 concentrations were then measured on a gas chromatograph (Thermo Scientific FOCUS GC) equipped with a HayeSep Q Packed GC Column and a flame ionization detector. A calibration curve was made using a certified 1000 ppm CH_4 standard (Scott Specialty Gases Netherlands B.V.). From the measured CH_4 concentration in the headspace, the total dissolved CH_4 in the bottom water was calculated using the equations in (Magen et al., 2014) with the Bunsen coefficient (Yamamoto et al., 1976). Benthic fluxes of DIC and CH_4 were calculated using the concentration changes of solutes in the bottom water of closed cores during the incubation period, as determined by linear regression analysis of the individual time series. Total organic matter mineralization was partitioned into aerobic and anaerobic contributions. Assuming a 1:1 stoichiometric relationship between O_2 consumption rate and DIC production rate for aerobic mineralization, the aerobic fraction was calculated from measured O_2 consumption, and the remaining OM-derived DIC production was attributed to anaerobic mineralization.

2.6. Subaerial incubation of dredged sediment

To investigate OM degradability under oxygen exposure during dredged sediment processing, open-air bottle incubations were conducted in triplicate for six sediments from sites that covered contrasting depositional and sedimentary conditions within the research area: three marine (115, 86, NWWG-02; Fig. 1a) and three riverine (21A, B16, K1v2; Fig. 1a), with differing sediment texture (silt-rich and sand-rich) in both groups. To obtain minimally altered sediment in which the water content could be accurately and rapidly adjusted, and to ensure reproducibility, we used freeze-dried and homogenized sediments from the six sites, in triplicate. The freeze-dried sediment was transferred into 330-mL borosilicate glass bottles, resulting in a thin sediment layer (< 5 mm). Artificial rainwater (composition in Table S1) was added to achieve a water content of 60% water-filled pore space (assuming the same porosity after rewetting; calculation provided in the SI), which is a water content optimal for soil respiration (Fairbairn et al., 2023). The rewetted sediments were incubated in the dark at room temperature (20 ℃). The CO_2 emission rates were measured on day 2, 6, 9, 16, 23, 30 and 37; in the later stages in incubations, the rates declined significantly and became relatively stable after around

314 one-month incubation, and the experiment was terminated. On the day of measurement, bottles were

315 sealed with rubber stoppers tightened with aluminum crimp caps for approximately 3 hours. We

316 measured the CO_2 concentrations in the headspace immediately after the bottles were capped and

317 approximately 3 hours later. The CO_2 accumulation in the headspace of each bottle during these 3

318 hours was used to calculate a CO_2 emission rate. For the rest of the time, bottles were kept open to

319 the atmosphere. The moisture level was maintained once a week and varied by less than 10% from

320 the target value.

321

322 The CO_2 measurement for the subaerial incubation was conducted by withdrawing a volume of 150

323 µL headspace gas using a 250-µL glass, gas-tight syringe (Hamilton). The headspace sample was

324 immediately injected into a gas chromatograph (GC, Agilent, 8890 GC system) equipped with a

325 Jetanizer and a flame ionization detector. Gases were carried by helium and separated by a

326 Carboxen-1010 PLOT analytical column (Sigma-Aldrich). Calibration was conducted by using certified

327 reference CO_2 gas (Scott specialty gases, Air Liquide, Eindhoven, The Netherlands).

328

329 To determine the percentage of degraded TOC over time, we firstly calculated the cumulative amount

330 of CO_2 emission and then normalized it to the total amount of organic carbon in the incubated

331 sediments, calculated from the dry sediment mass and its TOC content. The cumulative CO_2 emission

332 was obtained by integrating the CO_2 emission rate over time. For days when CO_2 emission rates were

333 not measured, the rates were estimated using spline interpolation. The integration and normalization

334 were performed using the 'AUC' (area under curve) function in RStudio.

335

336 **2.7. End-member modelling of OM sources**

337 Contributions of three major OM end-members (marine, riverine, and terrestrial) to the 49 sediments

338 were quantified based on $\delta^{13}C_{org}$ and C/N ratio using a Bayesian mixing model, MixSIAR (Stock et al.,

339 2018). Anthropogenic OM such as petroleum and coal products were not considered as they typically

340 have a much higher C/N ratio (Tumuluru et al., 2012) compared to the investigated samples here

341 (mostly <20), thus suggesting a limited contribution. Input from industrial and chemical waste is

342 considered being minimal because >90% of sediment is regarded as clean/safe with organic

343 contaminants below their national intervention values (Kirichek et al., 2018). We did not include

344 sewage OM and agricultural wastes as separate end-members due to their high variability in $\delta^{13}C_{org}$

345 (−28‰–−23‰; Shao et al., 2019) and C/N ratio (Chow et al., 2020; Puyuelo et al., 2011; Szulc et al.,

346 2021), and values largely overlaps with those of the considered three end-members. The model

347 incorporates the common ranges of three OM end-members in coastal environments (Table 1) and

348 employs Markov Chain Monte Carlo (MCMC) simulation to sample from the posterior distribution. The

349 distribution provides estimates of the mean contribution with standard deviation. The model was run in

350 RStudio with package "MixSIAR" integrated into the JAGS program.

351

Table 1. Mean values and standard deviations of $\delta^{13}C_{org}$ and C/N ratio of three OM end-members used in the MixSIAR analysis. Values from literature (Bianchi and Bauer, 2012; Finlay and Kendall, 2007; Lamb et al., 2006).

End-member	Typical OM	$\delta^{13}C_{org}$ (‰)	C/N
Marine OM end-member	Marine POC, algae, bacteria	−20±4	7±3
Riverine OM end-member	Freshwater POC, algae, bacteria	−29±4	7±3
Terrestrial OM end-member	Vegetation, soil OM, bacteria	−26.5±5.5	30±18

3. Results

3.1 Bulk geochemical feature of sediments

The PoR sediments were mostly (42 out of 49 samples) silt-rich with D50 smaller than 20 µm. A salinity gradient was observed in the study area increasing from approximately 0 at the most eastern part (Rotterdam city) to approximately 32 at the river mouth in the west. We observed a decrease in TOC content with increasing salinity (Fig. 2a). The silt-rich sediments generally contained more than 2.5 wt.% TOC, with significantly lower TOC contents in the sand-rich sediments ($p < 0.01$, Student's t-test). The weight ratio of C/N was between 5 and 13 for most samples (45 out of 49), and the corresponding $\delta^{13}C_{org}$ was in the range of -29‰ to -23‰ (Fig. 2b). Despite a weak correlation between C/N ratio and $\delta^{13}C_{org}$ ($R = -0.38$, Pearson), both properties showed (moderately) strong trends against salinity (C/N ratio: $R = -0.66$; $\delta^{13}C_{org}$: $R = 0.68$, Pearson; Fig. 2b).
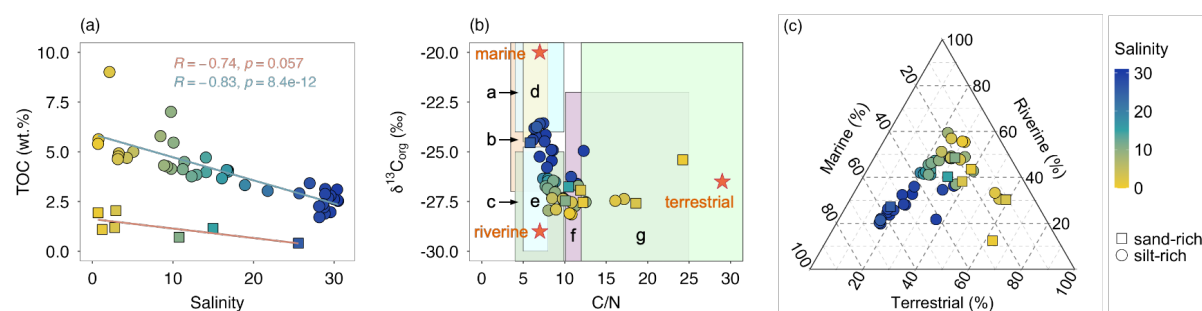

Fig. 2. Bulk geochemical properties of 49 sediment samples from the PoR. (a) TOC vs. salinity for both silt-rich (D50 < 20 µm) and sand-rich (D50 > 50 µm) sediments. (b) $\delta^{13}C_{org}$ and the weight ratio of C/N in sediments along salinity gradient in contrast to the typical $\delta^{13}C_{org}$ and C/N ranges for OM from coastal sediments in literature (Bianchi and Bauer, 2012; Finlay and Kendall, 2007; Lamb et al., 2006): **a** marine POC, **b** bacteria, **c** freshwater POC, **d** marine algae, **e** freshwater algae, **f** soil OM, **g** C3 terrestrial plants. Orange star symbols represent the mean values of three OM sources used in end-member analysis. (c) The contributions (%) of marine, riverine and terrestrial OM using a mixing model. The standard deviation (10–25%) is provided in the Supplementary Information (SI, Table S2).

3.2. Flash pyrolysis products of MOM

Pyrolysis of isolated MOM produced hundreds of pyrolysis compounds. The identified pyrolysis products are listed in Supplementary Information (Table S3). They were divided into nine groups based on the chemical characteristics, following the approach detailed in Nierop et al. (2017). Here in

382   Fig. 3, we present the relative abundance of six MOM pyrolysate groups along the salinity gradient,

383   including *n*-alkenes/alkanes, guaiacols, N-compounds, phenols, polysaccharide-derived products, and

384   syringols. The other three groups: phytadienes and pris-1-ene were only minor constituents (relative

385   abundance < 5%), and aromatics showed a negligible correlation with salinity ($-0.1 < R < 0.1$,

386   Pearson; Fig. S1). With increasing salinity, we observed an increase in the relative abundance of *n*-

387   alkenes/alkanes and N-compounds, while guaiacols, phenols, polysaccharides, and syringols

388   decreased. The correlations were generally moderate or weak, as suggested by the magnitude of the

389   correlation coefficient ($-0.6 < R < 0.6$, Pearson). Additionally, the correlation coefficients between the

390   identified MOM pyrolysate groups and other bulk sediment properties (i.e. D50, C/N, $\delta^{13}C_{org}$) were

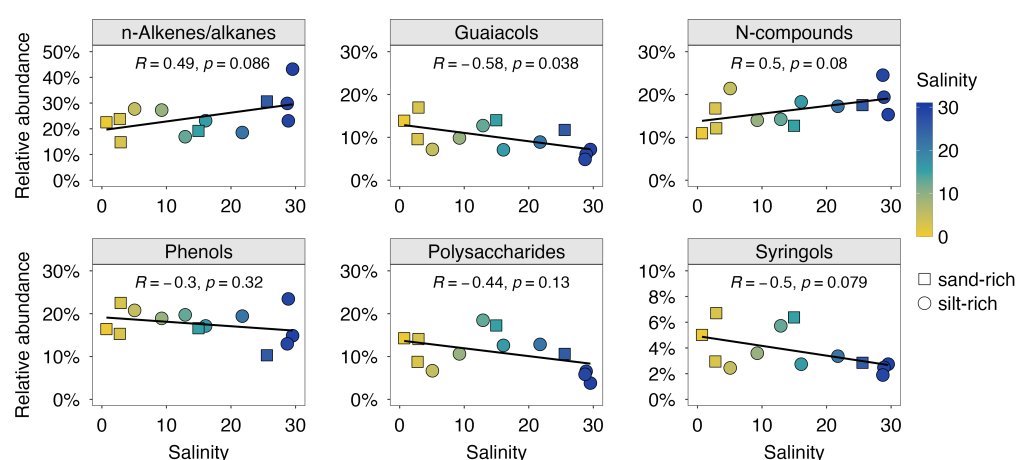391   also weak (see SI, Fig. S2).

392

393

394   **Figure 3.** The relative abundance of six groups of MOM pyrolysis products. Pearson correlation

395   coefficient (*R*) measures the strength of the linear relationship between grouped pyrolysates and

396   salinity.

397

398   **3.3. BIT index**

399   Crenarchaeol and branched GDGTs were detected in sediments from all 13 investigated sites. The

400   calculated BIT index ranged between 0.43 and 0.92 (Fig. 4a). A strong negative correlation was

401   observed between BIT index and salinity ($R = -0.88$, Pearson) and between BIT index and $\delta^{13}C_{org}$ (*R*

402    $= -0.83$, Pearson). In contrast, the correlations with MOM pyrolysis products were in general weak or

403   moderate ($-0.6 < R < 0.6$, Pearson; Fig. S2), except for guaiacols and N-compounds (Fig. 4b & 4c).

404   Additionally, we did not observe a significant difference between sand-rich and silt-rich sediments in
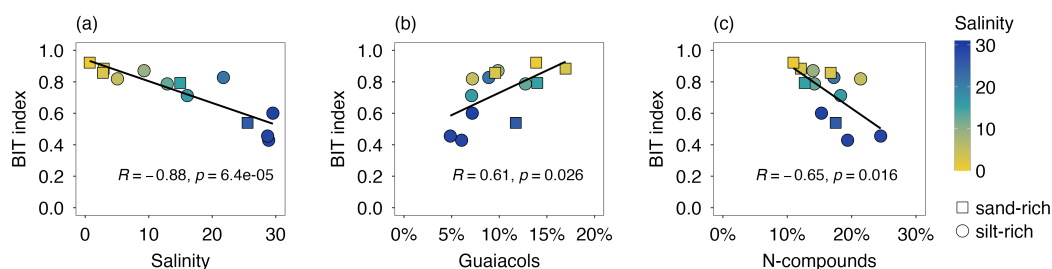
405   BIT index values ($p > 0.5$, Student's *t*-test).

406

Fig. 4. The BIT index of 13 sediments against (a) salinity, (b) relative abundance of guaiacols, (c) relative abundance of N-compounds.

3.4. Benthic fluxes on intact sediment cores

During the whole-core incubation, the O_2 concentration in the overlying water decreased linearly from around 90% to 60% air-saturation for both the high salinity location (115, salinity 29, later referred as 'marine' location) and the low salinity location (21A, salinity 5, later referred as 'riverine' location; SI Fig. S2). At the same time, concentrations of DIC and CH_4 in the overlying water increased linearly with time (Fig. S3). Benthic O_2 consumption and DIC release rates showed no significant differences between two contrasting locations ($p > 0.05$, Student's t-test), on average around 30 and 122–158 mmol m^{-2} d^{-1}, respectively (Fig. 5a, b). However, DIC was released into the overlying water at a much higher rate, 4–5 times larger than O_2 consumption rate. Correcting the DIC flux for contributions not associated with OM degradation (i.e. $CaCO_3$ dissolution) as described in the supplementary information provided us with an estimate of the DIC flux from OM degradation (DIC_{OM}) which accounted for 88–97% of the total DIC flux (Fig. 5c). When normalized to TOC to correct DIC_{OM} for differences in bulk TOC content, the DIC flux at 115 was about four times higher than at site 21A (Fig. 5d). Additionally, the CH_4 efflux was one to two orders of magnitude smaller than the O_2 and DIC fluxes and showed significant differences between two contrasting locations: the CH_4 efflux at the river location was more than five times higher compared to the marine location (Fig. 5e).
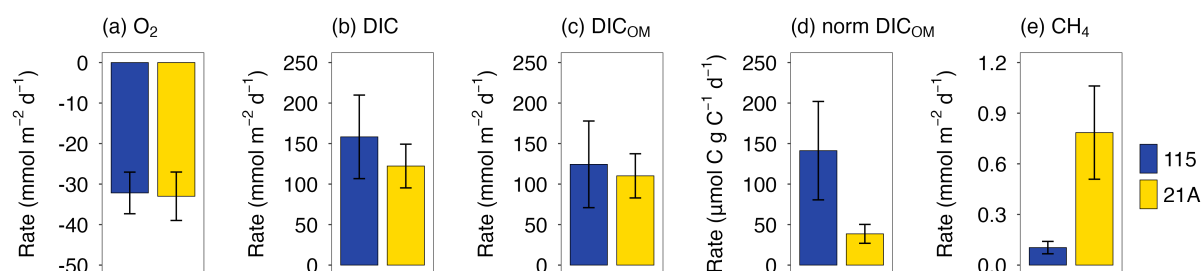

Fig. 5. Benthic fluxes of dissolved O_2 (a) and DIC (b) determined from whole-core incubation. Positive and negative rates represent efflux (from sediment into overlying water) and influx (from overlying water into sediment), respectively. The contribution of OM degradation to benthic DIC fluxes is shown in panel (c) and further normalized by sediment TOC in panel (d). Panel (e) shows benthic CH_4 fluxes. Error bars represent standard deviations from triplicate core incubations. Other measured fluxes (e.g. DIN, total alkalinity) are available in Fig. S4.

3.5. Subaerial carbon emissions from bulk sediments

During the aerobic incubation experiment, CO_2 accumulation was detected during the 3-hour rate measurements for all timesteps. The CO_2 emission rate, expressed as µg C g^{-1} day^{-1}, was the highest at the start of the incubation. Rates dropped drastically in the first two weeks and then stabilized after day 25. Here we present carbon emission rates at three timesteps representing the initial stage, declining stage, and stable stage (Fig. 6). The silt-rich sediments showed both higher emission rates throughout the incubation period (up to 120 µg C g^{-1} day^{-1}) and stronger decreases in rate over time (more than 60 µg C g^{-1} day^{-1}), compared to sand-rich sediments (maximum rate around 35 µg C g^{-1} day^{-1}; Fig. 6a). The TOC-normalized carbon emission rates were higher (up to three times) in the three marine sediments (salinity 27–28) compared to the three riverine sediments (salinity 0–5) throughout the experiment (Fig. 6b).
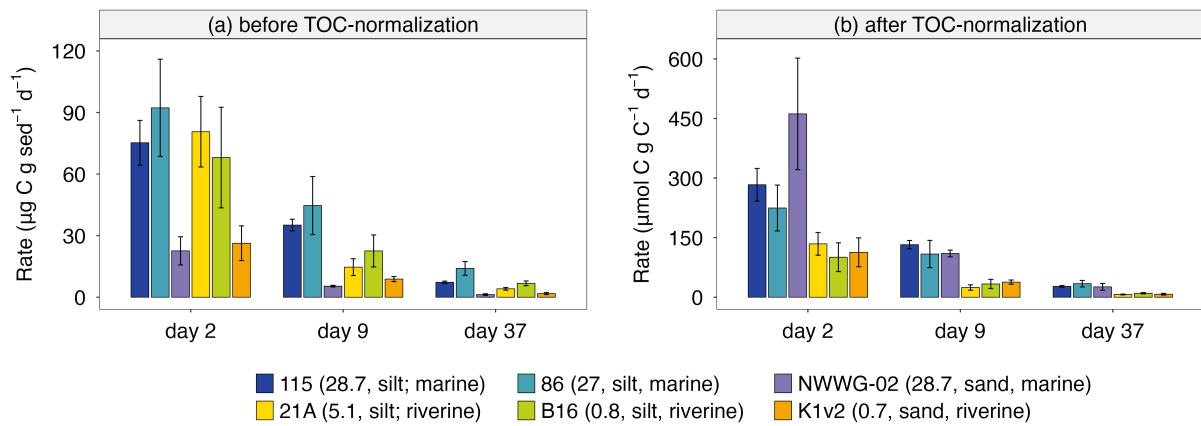

Fig. 6. Carbon emission rates in aerobic incubation at day 2, day 9 and day 37 from six sediments. Note the different scales and units for the y-axis for carbon emission rates before TOC-normalization (a) and after TOC-normalization (b). Site information (i.e. salinity, sediment texture, and marine/riverine location within the PoR) is given in brackets in the legend.

The decreasing trend of CO_2 emission rate was also reflected in the cumulative percentage of degraded TOC over time (Fig. 7), which increased fast initially and stabilized towards the end of the incubation experiment. After the 37-day incubation period, the amount of degraded TOC ranged from 1 to 7% for the investigated sites. Additionally, the percentage of degraded TOC was 2–4 times higher in sediments from marine locations than those in river locations, consistent with the differences in carbon emission rates (Fig. 6b).
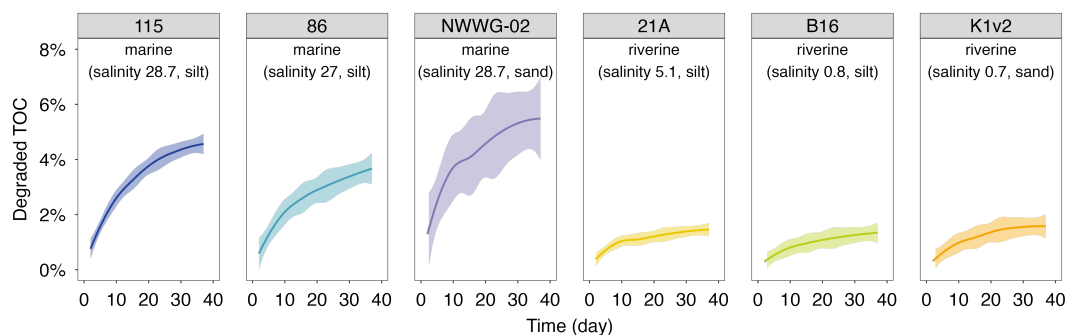
Fig. 7. The percentage of degraded TOC over time in aerobic incubation experiments. The shading areas represent the 95% confidential interval for the fitted locally estimated scatterplot smoothing (LOESS) curves.

4. Discussion

4.1 Organic matter content, source and composition in estuarine sediments

The PoR sediments are characterized by relatively high TOC contents compared to the North Sea surface sediments (0.03–2.79 wt.%; Wiesner et al., 1990), but in the range of Dutch coastal sediments (0–9.8 wt.%; Stronkhorst and Van Hattum, 2003) or other harbor systems such as the Port of Hamburg (2–7.6 wt.%; Zander et al., 2020). The high carbon content arose from high productivity and rapid burial of OM under high sedimentation rates; oxygen penetration is limited in rapidly accumulating, organic-rich sediment, and thus most OM breakdown occurs via relatively slow, anaerobic processes (Schulz and Zabel, 2006). Moreover, the fine sediment texture observed at most investigated sites limits oxygen diffusion and provides more sorption surface for OM (Keil et al., 1994), both contributing to the preservation of sedimentary OM and thus high TOC content compared to sandy sediment. This is expressed in the relatively low TOC content (0–2.5 wt.%) of the coarser-grained sediments shown in Fig. 2a. Besides the clear impact of grain size on OM content, a general decreasing trend in sediment TOC contents from river to marine area of the PoR sediments was observed, in line with previous work on estuarine sediment OM (Strong et al., 2012). The relatively low OM content in sediment from the marine-dominated sites in part arises from the large input (up to 5.7 million tons per year) in this area of repeatedly resuspended, OM-poor coastal sediment transported by strong tide and waves (Cox et al., 2021). More frequent dredging activities at the marine sites may also contribute to the lower OM content (Fig. 2a), as also witnessed in other coastal sediments (Aller et al., 1996). Furthermore, moving downstream from the riverine to the marine part of estuarine systems, the contribution of OM-rich riverine sediment not only decreases, but continuing OM degradation in this transported sediment further diminishes the amount of riverine OM (Bianchi et al., 2018; Freitas et al., 2021).

The OM burial and degradation are not only affected by the sediment dynamics as described above, but also by the source and inherent properties of the OM. The $\delta^{13}C_{org}$ and C/N ratio have been widely used to assess OM sources in coastal environments (Canuel and Hardison, 2016; Lamb et al., 2006;

15

Fig. 7. The percentage of degraded TOC over time in aerobic incubation experiments. The shading areas represent the 95% confidential interval for the fitted locally estimated scatterplot smoothing (LOESS) curves.

4. Discussion

4.1 Organic matter content, source and composition in estuarine sediments

The PoR sediments are characterized by relatively high TOC contents compared to the North Sea surface sediments (0.03–2.79 wt.%; Wiesner et al., 1990), but in the range of Dutch coastal sediments (0–9.8 wt.%; Stronkhorst and Van Hattum, 2003) or other harbor systems such as the Port of Hamburg (2–7.6 wt.%; Zander et al., 2020). The high carbon content arose from high productivity and rapid burial of OM under high sedimentation rates; oxygen penetration is limited in rapidly accumulating, organic-rich sediment, and thus most OM breakdown occurs via relatively slow, anaerobic processes (Schulz and Zabel, 2006). Moreover, the fine sediment texture observed at most investigated sites limits oxygen diffusion and provides more sorption surface for OM (Keil et al., 1994), both contributing to the preservation of sedimentary OM and thus high TOC content compared to sandy sediment. This is expressed in the relatively low TOC content (0–2.5 wt.%) of the coarser-grained sediments shown in Fig. 2a. Besides the clear impact of grain size on OM content, a general decreasing trend in sediment TOC contents from river to marine area of the PoR sediments was observed, in line with previous work on estuarine sediment OM (Strong et al., 2012). The relatively low OM content in sediment from the marine-dominated sites in part arises from the large input (up to 5.7 million tons per year) in this area of repeatedly resuspended, OM-poor coastal sediment transported by strong tide and waves (Cox et al., 2021). More frequent dredging activities at the marine sites may also contribute to the lower OM content (Fig. 2a), as also witnessed in other coastal sediments (Aller et al., 1996). Furthermore, moving downstream from the riverine to the marine part of estuarine systems, the contribution of OM-rich riverine sediment not only decreases, but continuing OM degradation in this transported sediment further diminishes the amount of riverine OM (Bianchi et al., 2018; Freitas et al., 2021).

The OM burial and degradation are not only affected by the sediment dynamics as described above, but also by the source and inherent properties of the OM. The $\delta^{13}C_{org}$ and C/N ratio have been widely used to assess OM sources in coastal environments (Canuel and Hardison, 2016; Lamb et al., 2006;

492 Li et al., 2021; Middelburg and Nieuwenhuize, 1998). The OM in the estuarine ecosystems can

493 originate from multiple sources, and the typical ranges of $\delta^{13}C_{org}$ and C/N ratio for the common OM

494 sources are indicated in Fig. 2b. The trends in $\delta^{13}C_{org}$ and C/N ratio suggest that OM in the PoR

495 sediments is derived from a mixture of marine, riverine and terrestrial OM that are sourced from algae,

496 bacteria, soil OM, and terrestrial plants, the relative contribution of these sources being a function of

497 depositional conditions (riverine versus marine) also reflected by salinity (Fig. 2b). The observed

498 $\delta^{13}C_{org}$ values (−29−−23‰) and their trend against salinity are similar to those in the broader Rhine

499 estuary reported in earlier work by (Middelburg and Herman, 2007), suggesting that intense sediment

500 reworking in connection with harbor expansion over the last 15 years has had little impact on

501 sediment OM sources. Furthermore, the range in observed $\delta^{13}C_{org}$ values is lower than that reported

502 for temperate marine OM (−18 and −22‰; Thornton and McManus, 1994), reflecting a significant non-

503 marine OM source even under nearly marine conditions at the river mouth. Quantification of the

504 different sources using end-member modelling similarly indicates that the dominant OM source shifts

505 with depositional environment: terrestrial OM in the most river-dominated locations (up to 65%,

506 salinity < 5), freshwater OM in the river-sea transitional area (~ 45%, 5 < salinity < 25), and marine

507 OM in the river-mouth area (up to 65%, salinity > 25).

508

509 Regarding the range of and trend in C/N values, it is important to note that the value is subject to OM-

510 specific alterations during sediment diagenesis: for higher plant litter, the C/N ratio decreases during

511 decomposition, while for aquatic detritus the C/N ratio increases during degradation (Hedges and

512 Oades, 1997; Wakeham and Canuel, 2006). These opposing diagenetic trajectories can result in a

513 convergence of C/N ratios of terrestrial and aquatic detritus (Middelburg and Herman, 2007). This

514 may explain the observation that bulk sediments at many of the investigated sites in the PoR research

515 area have C/N ratios near the upper limit of the typical range for freshwater algae (~8) or POC (~10),

516 or around the lower limit of the typical range for C_3 plants (~12, Fig. 2b). Compared to the C/N ratio,

517 the BIT index is thought to be less sensitive to diagenetic effects (Hopmans et al., 2004). This proxy

518 indicates a predominant riverine and/or terrestrial source of the sedimentary OM (Schouten et al.,

519 2013). The BIT values from this study are in line with the values previously determined by Herfort et

520 al. (2006) in sediment at Maassluis (0.74–0.82; close to NWWG-09, Fig 1), while they are much

521 higher than those determined in coastal sediments of the southern North Sea (0.02–0.25; Herfort et

522 al., 2006), highlighting the sharp transition in OM composition between estuarine and coastal systems

523 and the importance of non-marine OM throughout the harbor system.

524

525 The source proxies presented above ($\delta^{13}C_{org}$, C/N, BIT) indicate a strong terrestrial and riverine OM

526 signature across the salinity gradient in the PoR study area, with a considerable marine contribution

527 at the river mouth. The pyrolysis products from MOM offer additional insights into sediment OM

528 sources and composition. Guaiacols and syringols are pyrolytic markers of terrestrial OM, as they are

529 characteristic structural moieties of lignin, a typical biopolymer of higher plants. Their relative

530 abundance together (7–28%) falls within the reported lignin fractions (3–57%) for various coastal

531 aquatic environments (Brandini et al., 2022; Burdige, 2007; Kaal et al., 2020). Although having

532 multiple potential sources, the markers of polysaccharides in the investigated samples showed strong
533 positive correlations with both guaiacols (R = 0.77, Pearson) and syringols (R = 0.83, Pearson),
534 suggesting they were mainly derived from terrestrial higher plants. The decreasing trends of these
535 markers (relative abundance 10–40%) with increasing salinity, well aligned with $\delta^{13}C_{org}$ and BIT index,
536 further support the decreasing importance of terrestrial OM input towards the river mouth. In contrast,
537 N-compounds showed strong negative correlations with both guaiacols (R = −0.84, Pearson) and
538 syringols (R = −0.81, Pearson), suggesting a non-terrestrial OM origin such as protein from algal
539 detritus and chitin from various crustaceans (Nierop et al., 2017). *n*-Alkenes/alkanes, negatively
540 correlated with (terrestrial) polysaccharide-derived products (R = −0.78, Pearson; Fig. S2), were
541 probably from non-terrestrial sources like algaenan (de Leeuw et al., 2006). The other detected
542 pyrolysis products constituted a major fraction (> 50%) but most correlated with all mentioned source
543 proxies moderately or poorly (−0.5 < R < 0.5, Pearson; Fig. S2), thus are less effective provenance
544 proxies because they originate from multiple sources.
545
546 All proxies and analytical techniques have their strengths and weaknesses in determining OM
547 sources. Here, we obtain further insight into MOM characteristics by exploring the relationships
548 between different independent OM proxies and the end-member modelling results. There is a strong
549 agreement between the BIT index and the modelled non-marine OM contribution (R = 0.96, Pearson;
550 Fig. 8a), indicating that both approaches agree with respect to the relative contribution of terrestrial
551 sources (plants, rivers, soils) to the sedimentary OM pool. The contribution to the MOM pool by lignin-
552 derived products, likely representing remains of higher plants, was up to 40% (Fig. 8b) and correlated
553 strongly with BIT index (R = 0.62, Pearson). However, the weak slope in the scatter plot of BIT and
554 plant-MOM suggests that plant-derived OM was a lesser indicator of changes in OM composition and
555 reactivity in the harbor area. There was overall good agreement between the plant-derived
556 contribution from chemical MOM analysis and end-member modelling (Fig. 8c), indicating that mixing
557 models based on bulk OM parameters can provide valuable information about OM composition in
558 dynamic coastal settings.
559
560 The terrestrial OM fraction modelled from C/N and $\delta^{13}C_{org}$ showed a positive correlation with plant-
561 derived MOM pyrolysis products (Fig. 8c). Most data points seem to lie around the1:1 curve except for
562 two sand-rich outliers. However, interpreting their relationship in Fig. 8c is challenging because of the
563 complexity in assigning MOM pyrolysis products to terrestrial-derived OM in estuarine environments.
564 Phenols and N-compounds, partially derived from terrestrial OM, are not included in the presented
565 MOM-determined contribution here. On the other hand, pyrolysis of algal material also produces
566 polysaccharide-derived products (Stevenson and Abbott, 2019), which can lead to overestimation of
567 MOM-determined terrestrial contribution. Nevertheless, this study suggests using bulk proxies (C/N,
568 $\delta^{13}C_{org}$) in combination with biomarker proxies (BIT index, MOM pyrolysis products) can provide a
569 more complete picture of OM composition in highly dynamic systems like estuaries.
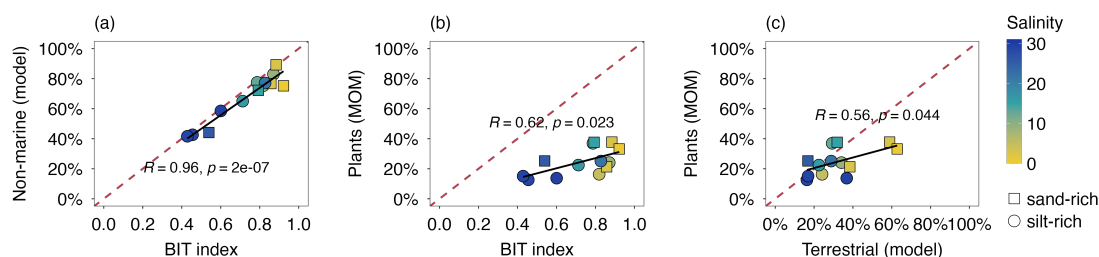570

Fig. 8. Scatter plots of proxies for OM source: (a) BIT index vs. non-marine OM contribution (i.e. terrestrial and riverine input from the three end-member modelling), (b) modelled terrestrial OM contribution vs. plant-derived MOM pyrolysis products (i.e. sum of guaiacols, syringols, polysaccharide-derived products), (c) BIT index vs. plant-derived MOM pyrolysis products (i.e. sum of guaiacols, syringols, polysaccharide-derived products). The red dashed lines are 1:1 curves and the black lines are the linear regression fitting curves.

4.2 Organic matter degradation: rates and pathways

In the 8-h whole-core incubation experiment, oxygen consumption was mostly due to OM mineralization; the upward diffusive fluxes of reduced species (e.g. Fe^{2+}, HS^-) that can react with oxygen represented a negligible oxygen sink at the sediment-water interface (< 1% of total oxygen uptake; calculation detailed in the SI). The measured benthic O_2 consumption rates in the PoR sediments (33 ± 6 mmol m^{-2} d^{-1}) were similar to the reported rates in coastal sediments in the North Sea (22.1 ± 0.6 mmol m^{-2} d^{-1}; Neumann et al., 2021) and other human-influenced estuarine sediments ($27–82$ mmol m^{-2} d^{-1}; Kraal et al., 2013). In estuarine systems, high primary production and shallow water depth (here 13–25 m) lead to deposition of a substantial amount of freshly produced OM, contributing to the high aerobic OM degradation rates. Furthermore, the whole-core incubation showed similar O_2 consumption rates between sediment types. However, TOC-normalized carbon emission rates from OM degradation—measured as DIC in the whole-core incubation and CO_2 in the subaerial bottle incubation experiment—were higher in marine sediments compared to riverine sediments (Fig. 5, 6). Here, the DIC_{OM} flux, which more broadly represents OM degradation in the surface sediment as it includes anaerobic OM degradation pathways, was normalized to TOC in order to compare between sites with strongly differing surface-sediment TOC contents (2.2 wt.% for site 115 vs. 5 wt.% for site 21A). The results indicate that short-term oxic respiration rates (Fig. 5a), driven by rapid degradation of freshly deposited (algal) OM at the sediment-water interface, were similar between sites. Furthermore, OM degradation rates may have been affected by (similar) limitation of O_2 supply rather than carbon availability. By contrast, overall (Fig. 5d) and long-term (Fig. 6b) OM degradation in the riverine sediment was 3–4 times slower than in the marine sediment, the former being characterized by a higher proportion of more recalcitrant OM sources. This suggests a link between OM composition and 'quality' (rather than quantity) and the CO_2 release potential from (dredged) estuarine sediment. Sediment from site 115 likely received a greater supply and burial of freshly produced (N-rich) algal OM, due to a faster burial rate (10–15 cm yr^{-1}) than at riverine site 21A (<10 cm yr^{-1}; Cox et al., 2021). Riverine sediments (e.g. 21A), however, were richer in eroded soil OM (Fig. 8), which is typically more recalcitrant and N-depleted than freshly produced algal OM.

606

607   Regarding the role of estuaries in carbon cycling, a crucial transition in anaerobic OM degradation

608   pathways is the onset of methanogenesis, which occurs when other TEAs have become depleted.

609   Due to a lower salinity and thus a shallowing of the sulfate-methane transition zone (Kuliński et al.,

610   2022), sediment from a river location (21A; salinity 5) exhibited an eight-time larger CH_4 efflux (Fig.

611   5c) compared to the marine location (115; salinity 29) despite of less degradable OM with a stronger

612   terrestrial signature (Fig. 2) as evidenced by the above-described lower OM mineralization rates

613   relative to TOC content. Similar spatial variability of benthic CH_4 fluxes as a function of salinity was

614   documented in other estuaries but with rather different values (0.2–19 mmol m^{-2} d^{-1}; Gelesh et al.,

615   2016; Li et al., 2021; Middelburg et al., 2002). Note that the benthic fluxes measured here do not

616   directly translate into atmospheric CO_2 and CH_4 emissions, as various processes (e.g. carbonate

617   system equilibria, CH_4 oxidation) act on the speciation and concentration of these greenhouse gases

618   released from the sediment. Nevertheless, estuaries are considered as hotspots for both CO_2 and

619   CH_4 emissions into atmosphere (Li et al., 2023; Middelburg et al., 2002). Therefore, elucidating how in

620   addition to OM content the source and composition as well environmental conditions during OM

621   degradation control the magnitude and speciation of carbon release from estuarine sediment is

622   important to better constrain the role of estuaries in global carbon cycling.

623

624   **4.3 The impact of perturbation on organic matter degradation**

625   Sediment dredging and its further management, such as relocation on land, often alter OM

626   degradation conditions substantially by reintroducing O_2. In principle, aerobic degradation is more

627   effective than anaerobic degradation as aerobic oxidation has a relatively high energy yield, especially

628   compared to sulfate reduction (Hansen and Blackburn, 1991). This is reflected in the whole-core

629   incubation results, where aerobic mineralization confined in the uppermost few-millimeter-thick

630   sediment layer (Revsbech et al., 1980) accounted for 25–30% of the total OM-derived DIC production

631   across the entire 15-cm sediment core. By manually perturbing sediments and exposing them to

632   atmospheric oxygen in subaerial incubations, we found that the initial (day 2) TOC-normalized carbon

633   emission rate (283±42 and 134±29 µmol C g C^{-1} d^{-1} for 115 and 21A, respectively; Fig. 6b) increased

634   to 2–3 times of that in undisturbed whole-core incubation (158±61 and 41±12 µmol C g C^{-1} d^{-1} for 115

635   and 21A, respectively; Fig. 5d). These findings agree with a slurry incubation experiment under

636   contrasting redox conditions using Dutch coastal sediments conducted by (Dauwe et al., 2001), which

637   showed that the mineralization rate under aerobic conditions was faster than anaerobic conditions by

638   up to one order of magnitude. Furthermore, the increase in carbon emission rate was more

639   pronounced in the riverine sediment (21A) with a three-fold increase after perturbation, compared to

640   the marine sediment (115) with a two-fold increase. We attribute this to the stronger terrestrial,

641   recalcitrant signature of OM in the riverine part of the investigated harbor area. (Hulthe et al., 1998)

642   suggested that the impact of redox conditions and specifically oxygen availability is greatest for

643   relatively recalcitrant OM; fresh, labile OM is degraded relatively rapidly under aerobic and anaerobic

644   conditions. Therefore, the difference in the observed rate increase following sediment perturbation

645   may be attributed to the more active enzymatic catalysis involved in the degradation of terrestrial OM,

646 such as lignin, cellulose, and tannins (Hedges and Oades, 1997), compared to freshly produced

647 marine OM was more predominant.

648

649 These OM source-dependent differences in OM degradation rates were expressed across the six

650 investigated sites: the TOC-normalized carbon emission rates were over 100% higher in marine

651 sediments (115, 86, NWWG-02) than riverine sediments (21A, B16, K1v2) at almost all timesteps (Fig.

652 6b). This observed difference was supported by the OM end-member analysis: sediments near the

653 river mouth (115, 86, NWWG-02) were composed of more than 50% marine OM and less than 20%

654 terrestrial OM, whereas sediments from the river side (21A, B16, K1v2) were dominated (>70%) by

655 non-marine OM (Fig. 2c, Table S2). The faster degradation rate of marine OM, such as algae, which

656 was reported to be up to 10 times faster than terrestrial OM (Guillemette et al., 2013), likely explains

657 the higher TOC-normalized carbon emission rates in marine sediments. We note that sample

658 treatment for the subaerial bottle incubation experiment, i.e. freeze-drying and rewetting, may have

659 reduced overall microbial activities and thus OM degradability, but previous studies indicate that such

660 an effect is likely limited (He et al., 2022; Wu et al., 2020) and does not affect the overall conclusions

661 regarding the role of OM source and reactivity in shaping CO_2 emission kinetics.

662

663 In addition to the degradation rate, the extent of OM degradation is also affected by the OM source

664 and composition. By the end of the subaerial incubation experiment, marine sediments (115, 86,

665 NWWG-02) exhibited 2–4 times larger fractions of degraded TOC than riverine sediments (21A, B16,

666 K1v2; Fig. 7). Despite a lower TOC content, marine sediments contained a higher percentage of

667 fresher and more labile OM, thus resulting in a larger biodegradation fraction after 37 days of

668 subaerial incubation. A majority of the annual dredged sediment volume is marine (~77%; Kirichek et

669 al., 2018) and, consequently, dredging mostly perturbs sediments with relatively labile OM and high

670 potential CO_2 emission rates. Interestingly, sand-rich sediment NWWG-02 exhibited a notably larger

671 biodegradable OM fraction (up to 7%; Fig. 7), highlighting sediment texture may play an important role

672 besides OM sources. Silt-rich sediment can contain 20 times more mineral-associated OM than sand-

673 rich wetland soils (Mirabito and Chambers, 2023). This mineral-associated OM, physically protected

674 by inorganic matrices from mineralization, was suggested to play a key role in lasting carbon

675 sequestration globally (Georgiou et al., 2022; Keil et al., 1994).

676

677 Despite variations in the fractions of degraded TOC, more than 90% of the organic carbon remained

678 in the sediments by the end of the 37-day aerobic incubation experiments (Fig. 7). This aligns with

679 other studies where a majority fraction (> 80%) of organic carbon remained preserved in sediments or

680 soils after prolonged incubation periods ranging from weeks to years (Gebert et al., 2019; Haynes,

681 2005; Plante et al., 2011). The predominant fraction of sediment OM being less degradable on such

682 timescales fits well with the relatively large amounts (~50%) of pyrolysis products derived from

683 (terrestrial) polysaccharide, *n*-alkenes/alkanes from algaenan, guaiacols and syringols from lignin.

684 However, (Zander et al., 2022) indicated that the slow degradation of the majority of OM could also be

685 attributed to its association with sedimentary minerals. Importantly, the remaining OM, while resistant

686   to degradation over weeks to years, is still potentially degradable on longer timescales and relevant

687   for the carbon footprint of perturbing estuarine sediment over decades. While the results in this study

688   indicate that reintroduction of O_2 leads to a short-lived increase in estuarine OM degradation rates,

689   the degradation can still be stimulated under certain conditions. For instance, the addition of fresh,

690   readily degradable OM, known as priming, was reported to increase the degradability of old,

691   recalcitrant OM by 59% (Huo et al., 2017). This highlights that the organic carbon turnover rate is

692   rather complex and can vary markedly under different sediment management practices.

693

694   **4.4 Implications and future perspectives**

695   Estuaries are sites of high OM production and understanding OM processes within these regions is

696   key to quantify organic carbon budgets along the river-estuary-coastal ocean continuum (Canuel and

697   Hardison, 2016). In the PoR, sediment OM degradation (i.e. degradation rate and biodegradable pool)

698   exhibited a large spatial variation (marine vs. riverine), demonstrated in both whole-core and subaerial

699   incubation experiments. This spatial variability likely reflected a shift of OM composition, where marine

700   sediment was richer in freshly produced, easily degradable OM of algal origin. Similar source-

701   dependent OM degradation patterns were also observed in other coastal systems (e.g. the Elbe

702   estuary; Zander et al., 2022). However, the spatial distribution of OM may vary between different

703   estuaries, driven by many environmental factors (e.g. hydrological conditions, nutrient availability, land

704   use). Combining multiple independent proxies (e.g. C/N, $\delta^{13}C_{org}$, biomarkers) can improve our ability

705   to understand the source, transport and fate of OM in (perturbed) estuarine environments.

706   Degradation of OM is responsible for nutrient cycling, oxygen balance between the aquatic system

707   and sediment, and most early diagenetic processes (Middelburg et al., 1993). Therefore, recognizing

708   and differentiating OM reactivity of varying sources can help to refine the biogeochemical processes

709   and minimize the uncertainty in estimating OM mineralization and preservation efficiency in both field

710   and theoretical frameworks.

711

712   Anthropogenic perturbation like dredging within the coastal zone have greatly intensified in recent

713   decades. It is therefore important to explore the impact of such activities, specifically dredging and

714   potential sediment reuse, on the fate of carbon stored in estuarine sediments. The growing trend of

715   sediment reuse on land (e.g. beach nourishment, dike construction) introduces subaerial conditions

716   that can boost carbon mineralization rates (2–3 times), as shown in the open-air incubations. Current

717   practice with unpolluted PoR dredged sediment is relocation in the shallow North Sea, which is likely

718   to lead to less CO_2 emission than open-air incubation because (1) burial of dredged sediment at sea

719   limits exposure to O_2 and thus degradation rates and (2) buffering of released CO_2 in the water

720   column by conversion to HCO_3^-. However, extensive resuspension in the coastal zone will increase

721   O_2 exposure and CO_2 release into seawater results in a pH decrease, and as such the reactivity of

722   dredged material as determined in this study is also relevant to inform about the environmental impact

723   of disposal at sea. Overall, balancing sediment valorization with its associated carbon footprint is of

724   importance in determining the suitable sediment management strategies.

725

726   Methane, a strong greenhouse gas, is often oversaturated in the OM-rich coastal sediments, favoring

727   CH_4 bubble formation. Most CH_4 is trapped below the sulfate-methane transition zone, within which

728   anaerobic oxidation of methane (AOM) coupled to SO_4^{2-} removes approximately 71% of the CH_4 in

729   marine sediments (Gao et al., 2022). Dredging, similar to the natural forms of sediment erosion (Hulot

730   et al., 2023), can disrupt the functioning of this AOM filter and destabilize riverbed/seabed, leading to

731   a temporary CH_4 escape via enhanced diffusion and ebullition (Maeck et al., 2013; Nijman et al.,

732   2022). However, in the long term, exposing sediments to oxygen is expected to inhibit methane

733   production and emissions (Nijman et al., 2022). Whether dredging and the following sediment

734   processing will shift the estuarine sediment from a carbon sink into a carbon source is dependent on

735   the pristine sediment carbon dynamics and the specifications of human disturbance. Indubitably,

736   estuaries will remain vulnerable to human pressure and climate change. These alternations will in

737   return influence the important drivers of the estuarine, further affecting the balance between OM

738   degradation and preservation (Heckbert et al., 2012).

739

740   **Conclusions**

741   The PoR sediments, like many other coastal sediments, exhibited relatively high OM content and

742   reactivity due to the high primary production and rapid sedimentation in these shallow aquatic

743   systems. Organic carbon in marine sediments degraded up to 5 times faster than that in riverine

744   sediments under both intact and perturbed conditions. This variability was suggested to reflect

745   differences in OM composition: marine sediments were richer in recently produced, labile algal OM.

746   By contrast, riverine sediments contained larger amounts of eroded, more recalcitrant soil and plant-

747   derived OM. Additionally, OM degradation rates were 2–3 times higher in the open-air, disturbed

748   sediment incubations than the intact whole-core incubations. This suggested that perturbation

749   triggered by sediment dredging and processing can mobilize the sequestered sediment organic

750   carbon. Despite only 1–7% of organic carbon was released after 37-day open-air incubation, certain

751   favorable conditions may still promote degradation of the remaining organic carbon. With the growing

752   need for dredging and other coastal sediment reworking, it is therefore of great importance to

753   consider the sensitivity of carbon in sediment management practices on relevant timescales and in

754   the context of the fast-changing environmental conditions.

755

756

757

758

767 **Data availability**

768 The datasets used in this study are available from the corresponding author upon reasonable request.

769

770 **Declaration of competing interest**

771 The authors declare no competing interests.

772

781

782 **Appendix A. Supplementary data**

783 The online version contains supplementary material available at XXX.

784

785

786

787 **References**

788 Aller, R. C.: Bioturbation and remineralization of sedimentary organic matter: effects of redox
789 oscillation, Chem Geol, 114, 331–345, https://doi.org/10.1016/0009-2541(94)90062-0, 1994.

790 Amar, M., Benzerzour, M., Kleib, J., and Abriak, N. E.: From dredged sediment to supplementary
791 cementitious material: characterization, treatment, and reuse, International Journal of Sediment
792 Research, 36, 92–109, https://doi.org/10.1016/j.ijsrc.2020.06.002, 2021.

793 Arndt, S., Jørgensen, B. B., LaRowe, D. E., Middelburg, J. J., Pancost, R. D., and Regnier, P.:
794 Quantifying the degradation of organic matter in marine sediments: A review and synthesis, Earth Sci
795 Rev, 123, 53–86, https://doi.org/10.1016/j.earscirev.2013.02.008, 2013.

796 Barbier, E. B., Hacker, S. D., Kennedy, C., Koch, E. W., Stier, A. C., and Silliman, B. R.: The value of
797 estuarine and coastal ecosystem services, Ecol Monogr, 81, 169–193, https://doi.org/10.1890/10-
798 1510.1, 2011.

799 Bauer, J. E., Cai, W. J., Raymond, P. A., Bianchi, T. S., Hopkinson, C. S., and Regnier, P. A. G.: The
800 changing carbon cycle of the coastal ocean, Nature, 504, 61–70, https://doi.org/10.1038/nature12857,
801 2013.

802 Bianchi, T. S. and Bauer, J. E.: Particulate Organic Carbon Cycling and Transformation, Elsevier Inc.,
803 69–117 pp., https://doi.org/10.1016/B978-0-12-374711-2.00503-9, 2012.

804 Bianchi, T. S., Cui, X., Blair, N. E., Burdige, D. J., Eglinton, T. I., and Galy, V.: Centers of organic
805 carbon burial and oxidation at the land-ocean interface, Org Geochem, 115, 138–155,
806 https://doi.org/10.1016/j.orggeochem.2017.09.008, 2018.

807 Brandini, N., da Costa Machado, E., Sanders, C. J., Cotovicz, L. C., Bernardes, M. C., and Knoppers,
808 B. A.: Organic matter processing through an estuarine system: Evidence from stable isotopes (δ13C
809 and δ15N) and molecular (lignin phenols) signatures, Estuar Coast Shelf Sci, 265,
810 https://doi.org/10.1016/j.ecss.2021.107707, 2022.

811 Burd, A. B., Frey, S., Cabre, A., Ito, T., Levine, N. M., Lønborg, C., Long, M., Mauritz, M., Thomas, R.
812 Q., Stephens, B. M., Vanwalleghem, T., and Zeng, N.: Terrestrial and marine perspectives on
813 modeling organic matter degradation pathways, Glob Chang Biol, 22, 121–136,
814 https://doi.org/10.1111/gcb.12987, 2016.

815 Burdige, D. J.: Preservation of organic matter in marine sediments: Controls, mechanisms, and an
816 imbalance in sediment organic carbon budgets?, Chem Rev, 107, 467–485,
817 https://doi.org/10.1021/cr050347q, 2007.

818 Burdige, D. J.: Estuarine and Coastal Sediments - Coupled Biogeochemical Cycling, Elsevier Inc.,
819 279–316 pp., https://doi.org/10.1016/B978-0-12-374711-2.00511-8, 2012.

820 Buurman, P., Nierop, K. G. J., Pontevedra-Pombal, X., and Martínez Cortizas, A.: Chapter 10
821 Molecular chemistry by pyrolysis-GC/MS of selected samples of the Penido Vello peat deposit,
822 Galicia, NW Spain, Developments in Earth Surface Processes, 9, 217–240,
823 https://doi.org/10.1016/S0928-2025(06)09010-9, 2006.

824 Canuel, E. A. and Hardison, A. K.: Sources, Ages, and Alteration of Organic Matter in Estuaries, Ann
825 Rev Mar Sci, 8, 409–434, https://doi.org/10.1146/annurev-marine-122414-034058, 2016.

826 Cao, C., Cai, F., Qi, H., Zhao, S., and Wu, C.: Differences in the sulfate–methane transitional zone in
827 coastal pockmarks in various sedimentary environments, Water (Switzerland), 13, 1–18,
828 https://doi.org/10.3390/w13010068, 2021.

829 Carneiro, L. M., do Rosário Zucchi, M., de Jesus, T. B., da Silva Júnior, J. B., and Hadlich, G. M.:
830 δ13C, δ15N and TOC/TN as indicators of the origin of organic matter in sediment samples from the
831 estuary of a tropical river, Mar Pollut Bull, 172, https://doi.org/10.1016/j.marpolbul.2021.112857, 2021.

832 Chow, W. L., Chong, S., Lim, J. W., Chan, Y. J., Chong, M. F., Tiong, T. J., Chin, J. K., Pan, G. T.,
833 Puyuelo, B., Ponsá, S., Gea, T., Sánchez, A., Szulc, W., Rutkowska, B., Gawroński, S., and
834 Wszelaczyńska, E.: Determining C/N ratios for typical organic wastes using biodegradable fractions,
835 Processes, 85, 653–659, https://doi.org/10.3390/pr9091501, 2020.

836 Cloern, J. E., Canuel, E. A., and Harris, D.: Stable carbon and nitrogen isotope composition of aquatic
837 and terrestrial plants of the San Francisco Bay estuarine system, Limnol Oceanogr, 47, 713–729,
838 https://doi.org/10.4319/lo.2002.47.3.0713, 2002.

839 Cox, J. R., Dunn, F. E., Nienhuis, J. H., van der Perk, M., and Kleinhans, M. G.: Climate change and
840 human influences on sediment fluxes and the sediment budget of an urban delta: The example of the

841   lower rhine–meuse delta distributary network, Anthropocene Coasts, 4, 251–280,
842   https://doi.org/10.1139/anc-2021-0003, 2021.

843   Dauwe, B., Middelburg, J. J., and Herman, P. M. J.: Effect of oxygen on the degradability of organic
844   matter in subtidal and intertidal sediments of the North Sea area, 215, 13–22, 2001.

845   Dürr, H. H., Laruelle, G. G., van Kempen, C. M., Slomp, C. P., Meybeck, M., and Middelkoop, H.:
846   Worldwide Typology of Nearshore Coastal Systems: Defining the Estuarine Filter of River Inputs to
847   the Oceans, Estuaries and Coasts, 34, 441–458, https://doi.org/10.1007/s12237-011-9381-y, 2011.

848   Egger, M., Riedinger, N., Mogollón, J. M., and Jørgensen, B. B.: Global diffusive fluxes of methane in
849   marine sediments, Nat Geosci, 11, 421–425, https://doi.org/10.1038/s41561-018-0122-8, 2018.

850   Fabbri, D., Sangiorgi, F., and Vassura, I.: Pyrolysis-GC-MS to trace terrigenous organic matter in
851   marine sediments: A comparison between pyrolytic and lipid markers in the Adriatic Sea, Anal Chim
852   Acta, 530, 253–261, https://doi.org/10.1016/j.aca.2004.09.020, 2005.

853   Fairbairn, L., Rezanezhad, F., Gharasoo, M., Parsons, C. T., Macrae, M. L., Slowinski, S., and Van
854   Cappellen, P.: Relationship between soil CO_2 fluxes and soil moisture: Anaerobic sources explain
855   fluxes at high water content, Geoderma, 434, 116493,
856   https://doi.org/10.1016/j.geoderma.2023.116493, 2023.

857   Finlay, J. C. and Kendall, C.: Stable Isotope Tracing of Temporal and Spatial Variability in Organic
858   Matter Sources to Freshwater Ecosystems, in: Stable Isotopes in Ecology and Environmental
859   Science, edited by: Michener, R. and Lajtha, Wiley, 283–333,
860   https://doi.org/10.1002/9780470691854.ch10, 2007.

861   Freitas, F. S., Pika, P. A., Kasten, S., Jorgensen, B. B., Rassmann, J., Rabouille, C., Thomas, S.,
862   Sass, H., Pancost, R. D., and Arndt, S.: New insights into large-scale trends of apparent organic
863   matter reactivity in marine sediments and patterns of benthic carbon transformation, Biogeosciences,
864   18, 4651–4679, https://doi.org/10.5194/bg-18-4651-2021, 2021.

865   Gao, Y., Wang, Y., Lee, H. S., and Jin, P.: Significance of anaerobic oxidation of methane (AOM) in
866   mitigating methane emission from major natural and anthropogenic sources: a review of AOM rates in
867   recent publications, Environmental Science: Advances, 1, 401–425,
868   https://doi.org/10.1039/d2va00091a, 2022.

869   Gebert, J., Knoblauch, C., and Gröngröft, A.: Gas production from dredged sediment, Waste
870   Management, 85, 82–89, https://doi.org/10.1016/j.wasman.2018.12.009, 2019.

871   Gelesh, L., Marshall, K., Boicourt, W., and Lapham, L.: Methane concentrations increase in bottom
872   waters during summertime anoxia in the highly eutrophic estuary, Chesapeake Bay, U.S.A., Limnol
873   Oceanogr, 61, S253–S266, https://doi.org/10.1002/lno.10272, 2016.

874   Georgiou, K., Jackson, R. B., Vindušková, O., Abramoff, R. Z., Ahlström, A., Feng, W., Harden, J. W.,
875   Pellegrini, A. F. A., Polley, H. W., Soong, J. L., Riley, W. J., and Torn, M. S.: Global stocks and
876   capacity of mineral-associated soil organic carbon, Nat Commun, 13, 1–12,
877   https://doi.org/10.1038/s41467-022-31540-9, 2022.

878   Guillemette, F., McCallister, S. L., and Del Giorgio, P. A.: Differentiating the degradation dynamics of
879   algal and terrestrial carbon within complex natural dissolved organic carbon in temperate lakes, J
880   Geophys Res Biogeosci, 118, 963–973, https://doi.org/10.1002/jgrg.20077, 2013.

881   Hansen, L. S. and Blackburn, T. H.: Aerobic and anaerobic mineralization of organic material in
882   marine sediment microcosms, Mar Ecol Prog Ser, 75, 283–291, https://doi.org/10.3354/meps075283,
883   1991.

884   Haynes, R. J.: Labile Organic Matter Fractions as Central Components of the Quality of Agricultural
885   Soils: An Overview, Advances in Agronomy, 85, 221–268, https://doi.org/10.1016/S0065-
886   2113(04)85005-3, 2005.

887   He, Y., Zhang, T., Zhao, Q., Gao, X., He, T., and Yang, S.: Response of GHG emissions to interactions
888   of temperature and drying in the karst wetland of the Yunnan-Guizhou Plateau, Front Environ Sci, 10,
889   https://doi.org/10.3389/fenvs.2022.973900, 2022.

890   Heckbert, S., Costanza, R., Poloczanska, E. S., and Richardson, A. J.: Climate Regulation as a
891   Service from Estuarine and Coastal Ecosystems, Elsevier Inc., 199–216 pp.,
892   https://doi.org/10.1016/B978-0-12-374711-2.01211-0, 2012.

893   Hedges, J. I. and Oades, J. M.: Comparative organic geochemistries of soils and marine sediments,
894   Org Geochem, 27, 319–361, https://doi.org/10.1016/S0146-6380(97)00056-9, 1997.

Herfort, L., Schouten, S., Boon, J. P., Woltering, M., Baas, M., Weijers, J. W. H., and Sinninghe Damsté, J. S.: Characterization of transport and deposition of terrestrial organic matter in the southern North Sea using the BIT index, Limnol Oceanogr, 51, 2196–2205, https://doi.org/10.4319/lo.2006.51.5.2196, 2006.

Holligan, P. M. and Reiners, W. A.: Predicting the Responses of the Coastal Zone to Global Change, Adv Ecol Res, 22, 211–255, https://doi.org/10.1016/S0065-2504(08)60137-3, 1992.

Hopmans, E. C., Weijers, J. W. H., Schefuß, E., Herfort, L., Sinninghe Damsté, J. S., and Schouten, S.: A novel proxy for terrestrial organic matter in sediments based on branched and isoprenoid tetraether lipids, Earth Planet Sci Lett, 224, 107–116, https://doi.org/10.1016/j.epsl.2004.05.012, 2004.

Hopmans, E. C., Schouten, S., and Sinninghe Damsté, J. S.: The effect of improved chromatography on GDGT-based palaeoproxies, Org Geochem, 93, 1–6, https://doi.org/10.1016/j.orggeochem.2015.12.006, 2016.

Hulot, V., Metzger, E., Thibault de Chanvalon, A., Mouret, A., Schmidt, S., Deflandre, B., Rigaud, S., Beneteau, E., Savoye, N., Souchu, P., Le Merrer, Y., and Maillet, G. M.: Impact of an exceptional winter flood on benthic oxygen and nutrient fluxes in a temperate macrotidal estuary: Potential consequences on summer deoxygenation, Front Mar Sci, 10, https://doi.org/10.3389/fmars.2023.1083377, 2023.

Hulthe, G., Hulth, S., and Hall, P. O. J.: Effect of oxygen on degradation rate of refractory and labile organic matter in continental margin sediments, Geochim Cosmochim Acta, 62, 1319–1328, https://doi.org/10.1016/S0016-7037(98)00044-1, 1998.

Huo, C., Luo, Y., and Cheng, W.: Rhizosphere priming effect: A meta-analysis, Soil Biol Biochem, 111, 78–84, https://doi.org/10.1016/j.soilbio.2017.04.003, 2017.

Hutchings, J. A., Bianchi, T. S., Najjar, R. G., Herrmann, M., Kemp, W. M., Hinson, A. L., and Feagin, R. A.: Carbon Deposition and Burial in Estuarine Sediments of the Contiguous United States, Global Biogeochem Cycles, 34, https://doi.org/10.1029/2019GB006376, 2020.

IJsseldijk, L. L., Camphuysen, K. C. J., Nauw, J. J., and Aarts, G.: Going with the flow: Tidal influence on the occurrence of the harbour porpoise (Phocoena phocoena) in the Marsdiep area, The Netherlands, J Sea Res, 103, 129–137, https://doi.org/10.1016/j.seares.2015.07.010, 2015.

Jørgensen, B. B., Wenzhöfer, F., Egger, M., and Glud, R. N.: Sediment oxygen consumption: Role in the global marine carbon cycle, Earth Sci Rev, 228, https://doi.org/10.1016/j.earscirev.2022.103987, 2022.

Kaal, J.: Analytical pyrolysis in marine environments revisited, Analytical Pyrolysis Letters, 1–16, 2019.

Kaal, J., Martínez Cortizas, A., Mateo, M. Á., and Serrano, O.: Deciphering organic matter sources and ecological shifts in blue carbon ecosystems based on molecular fingerprinting, Science of the Total Environment, 742, 140554, https://doi.org/10.1016/j.scitotenv.2020.140554, 2020.

Keil, R., Montluçon, D., Prahl, F., and Hedges, J.: Sorptive preservation of labile organic matter in marine sediments, Nature, 370, 549–552, https://doi.org/https://doi-org.utrechtuniversity.idm.oclc.org/10.1038/370549a0, 1994.

Kirichek, A., Rutgers, R., Wensween, M., and van Hassent, A.: Sediment management in the Port of Rotterdam, in: Baggern - Unterbringen - Aufbereiten - Verwerten, Steinbeis-Transverzentrum Angewandte Landschaftsplanung, 1–8, 2018.

Kraal, P., Burton, E. D., Rose, A. L., Cheetham, M. D., Bush, R. T., and Sullivan, L. A.: Decoupling between water column oxygenation and benthic phosphate dynamics in a shallow eutrophic estuary, Environ Sci Technol, 47, 3114–3121, https://doi.org/10.1021/es304868t, 2013.

Kuliński, K., Rehder, G., Asmala, E., Bartosova, A., Carstensen, J., Gustafsson, B., Hall, P. O. J., Humborg, C., Jilbert, T., Jürgens, K., Meier, H. E. M., Müller-Karulis, B., Naumann, M., Olesen, J. E., Savchuk, O., Schramm, A., Slomp, C. P., Sofiev, M., Sobek, A., Szymczycha, B., and Undeman, E.: Biogeochemical functioning of the Baltic Sea, https://doi.org/10.5194/esd-13-633-2022, 2022.

Kuwae, T., Kanda, J., Kubo, A., Nakajima, F., Ogawa, H., Sohma, A., and Suzumura, M.: Blue carbon in human-dominated estuarine and shallow coastal systems, Ambio, 45, 290–301, https://doi.org/10.1007/s13280-015-0725-x, 2016.

Lamb, A. L., Wilson, G. P., and Leng, M. J.: A review of coastal palaeoclimate and relative sea-level reconstructions using $\delta 13C$ and C/N ratios in organic material, Earth Sci Rev, 75, 29–57, https://doi.org/10.1016/j.earscirev.2005.10.003, 2006.

950 LaRowe, D. E. and Van Cappellen, P.: Degradation of natural organic matter: A thermodynamic
951 analysis, Geochim Cosmochim Acta, 75, 2030–2042, https://doi.org/10.1016/j.gca.2011.01.020, 2011.

952 LaRowe, D. E., Arndt, S., Bradley, J. A., Estes, E. R., Hoarfrost, A., Lang, S. Q., Lloyd, K. G.,
953 Mahmoudi, N., Orsi, W. D., Shah Walter, S. R., Steen, A. D., and Zhao, R.: The fate of organic carbon
954 in marine sediments - New insights from recent data and analysis, Earth Sci Rev, 204, 103146,
955 https://doi.org/10.1016/j.earscirev.2020.103146, 2020.

956 Laruelle, G. G., Dürr, H. H., Slomp, C. P., and Borges, A. V.: Evaluation of sinks and sources of CO2
957 in the global coastal ocean using a spatially-explicit typology of estuaries and continental shelves,
958 Geophys Res Lett, 37, 1–6, https://doi.org/10.1029/2010GL043691, 2010.

959 de Leeuw, J. W., Versteegh, G. J. M., and van Bergen, P. F.: Biomacromolecules of algae and plants
960 and their fossil analogues, Plant Ecol, 182, 209–233, https://doi.org/10.1007/s11258-005-9027-x,
961 2006.

962 Li, M., Guo, Y., Cai, W. J., Testa, J. M., Shen, C., Li, R., and Su, J.: Projected increase in carbon
963 dioxide drawdown and acidification in large estuaries under climate change, Commun Earth Environ,
964 4, 1–10, https://doi.org/10.1038/s43247-023-00733-5, 2023.

965 Li, Y., Zhan, L., Chen, L., Zhang, J., Wu, M., and Liu, J.: Spatial and temporal patterns of methane
966 and its influencing factors in the Jiulong River estuary, southeastern China, Mar Chem, 228, 103909,
967 https://doi.org/10.1016/j.marchem.2020.103909, 2021.

968 Lovley, D. R. and Phillips, E. J. P.: Availability of Ferric Iron for Microbial Reduction in Bottom
969 Sediments of the Freshwater Tidal Potomac River, Appl Environ Microbiol, 52,
970 https://doi.org/https://doi.org/10.1128/aem.52.4.751-757.1986, 1986.

971 Macreadie, P. I., Anton, A., Raven, J. A., Beaumont, N., Connolly, R. M., Friess, D. A., Kelleway, J. J.,
972 Kennedy, H., Kuwae, T., Lavery, P. S., Lovelock, C. E., Smale, D. A., Apostolaki, E. T., Atwood, T. B.,
973 Baldock, J., Bianchi, T. S., Chmura, G. L., Eyre, B. D., Fourqurean, J. W., Hall-Spencer, J. M.,
974 Huxham, M., Hendriks, I. E., Krause-Jensen, D., Laffoley, D., Luisetti, T., Marbà, N., Masque, P.,
975 McGlathery, K. J., Megonigal, J. P., Murdiyarso, D., Russell, B. D., Santos, R., Serrano, O., Silliman,
976 B. R., Watanabe, K., and Duarte, C. M.: The future of Blue Carbon science, Nat Commun, 10, 1–13,
977 https://doi.org/10.1038/s41467-019-11693-w, 2019.

978 Maeck, A., Delsontro, T., McGinnis, D. F., Fischer, H., Flury, S., Schmidt, M., Fietzek, P., and Lorke, A.:
979 Sediment trapping by dams creates methane emission hot spots, United States of America,
980 Environmental Science and Technology, 8130–8137, 2013.

981 Magen, C., Lapham, L. L., Pohlman, J. W., Marshall, K., Bosman, S., Casso, M., and Chanton, J. P.: A
982 simple headspace equilibration method for measuring dissolved methane, Limnol Oceanogr Methods,
983 12, 637–650, https://doi.org/10.4319/lom.2014.12.637, 2014.

984 McLeod, E., Chmura, G. L., Bouillon, S., Salm, R., Björk, M., Duarte, C. M., Lovelock, C. E.,
985 Schlesinger, W. H., and Silliman, B. R.: A blueprint for blue carbon: Toward an improved
986 understanding of the role of vegetated coastal habitats in sequestering CO2, Front Ecol Environ, 9,
987 552–560, https://doi.org/10.1890/110004, 2011.

988 Middelburg, J. J. and Herman, P. M. J.: Organic matter processing in tidal estuaries, Mar Chem, 106,
989 127–147, https://doi.org/10.1016/j.marchem.2006.02.007, 2007.

990 Middelburg, J. J. and Nieuwenhuize, J.: Carbon and nitrogen stable isotopes in suspended matter and
991 sediments from the Schelde Estuary, Mar Chem, 60, 217–225, https://doi.org/10.1016/S0304-
992 4203(97)00104-7, 1998.

993 Middelburg, J. J., Vlug, T., Jaco, F., and van der Nat, W. A.: Organic matter mineralization in marine
994 systems, Glob Planet Change, 8, 47–58, https://doi.org/10.1016/0921-8181(93)90062-S, 1993.

995 Middelburg, J. J., Nieuwenhuize, J., Iversen, N., Høgh, N., De Wilde, H., Helder, W., Seifert, R., and
996 Christof, O.: Methane distribution in European tidal estuaries, Biogeochemistry, 59, 95–119,
997 https://doi.org/10.1023/A:1015515130419, 2002.

998 Mirabito, A. J. and Chambers, L. G.: Quantifying mineral-associated organic matter in wetlands as an
999 indicator of the degree of soil carbon protection, Geoderma, 430, 116327,
1000 https://doi.org/10.1016/j.geoderma.2023.116327, 2023.

1001 Neumann, A., van Beusekom, J. E. E., Eisele, A., Emeis, K. C., Friedrich, J., Kröncke, I., Logemann,
1002 E. L., Meyer, J., Naderipour, C., Schückel, U., Wrede, A., and Zettler, M. L.: Macrofauna as a major
1003 driver of bentho-pelagic exchange in the southern North Sea, Limnol Oceanogr, 66, 2203–2217,
1004 https://doi.org/10.1002/lno.11748, 2021.

1005 Nierop, K. G. J., Reichart, G. J., Veld, H., and Sinninghe Damsté, J. S.: The influence of oxygen
1006 exposure time on the composition of macromolecular organic matter as revealed by surface
1007 sediments on the Murray Ridge (Arabian Sea), Geochim Cosmochim Acta, 206, 40–56,
1008 https://doi.org/10.1016/j.gca.2017.02.032, 2017.

1009 Nijman, T. P. A., Lemmens, M., Lurling, M., Kosten, S., Welte, C., and Veraart, A. J.: Phosphorus
1010 control and dredging decrease methane emissions from shallow lakes, Science of the Total
1011 Environment, 847, 157584, https://doi.org/10.1016/j.scitotenv.2022.157584, 2022.

1012 Plante, A. F., Fernández, J. M., Haddix, M. L., Steinweg, J. M., and Conant, R. T.: Biological, chemical
1013 and thermal indices of soil organic matter stability in four grassland soils, Soil Biol Biochem, 43,
1014 1051–1058, https://doi.org/10.1016/j.soilbio.2011.01.024, 2011.

1015 Puyuelo, B., Ponsá, S., Gea, T., and Sánchez, A.: Determining C/N ratios for typical organic wastes
1016 using biodegradable fractions, Chemosphere, 85, 653–659,
1017 https://doi.org/10.1016/j.chemosphere.2011.07.014, 2011.

1018 Revsbech, N. P., Sorensen, J., Blackburn, T. H., and Lomholt, J. P.: Distribution of oxygen in marine
1019 sediments measured with microelectrodes, Limnol Oceanogr, 25, 403–411,
1020 https://doi.org/10.4319/lo.1980.25.3.0403, 1980.

1021 Schouten, S., Hopmans, E. C., and Sinninghe Damsté, J. S.: The organic geochemistry of glycerol
1022 dialkyl glycerol tetraether lipids: A review, Org Geochem, 54, 19–61,
1023 https://doi.org/10.1016/j.orggeochem.2012.09.006, 2013.

1024 Schulz, H. and Zabel, M.: Marine Geochemistry, Springer Berlin Heidelberg New York, 132 pp., 2006.

1025 Shao, L., Wu, D., Zhang, D., and Feng, T.: Using Isotopes to Identify the Sources of Organic Carbon
1026 and Nitrogen in Surface Sediment in Shallow Lakes Alongside Poyang Lake, Wetlands, 39, 25–33,
1027 https://doi.org/10.1007/s13157-017-0988-z, 2019.

1028 Smith, R. W., Bianchi, T. S., and Savage, C.: Comparison of lignin phenols and branched/isoprenoid
1029 tetraethers (BIT index) as indices of terrestrial organic matter in Doubtful Sound, Fiordland, New
1030 Zealand, Org Geochem, 41, 281–290, https://doi.org/10.1016/j.orggeochem.2009.10.009, 2010.

1031 Steele, J. H., Thorpe, S. A., and Turekian, K. K.: Marine Chemistry & Geochemistry, edited by: Steele,
1032 J. H., Thorpe, S. A., and Turekian, K. K., 2010.

1033 Stevenson, M. A. and Abbott, G. D.: Exploring the composition of macromolecular organic matter in
1034 Arctic Ocean sediments under a changing sea ice gradient, J Anal Appl Pyrolysis, 140, 102–111,
1035 https://doi.org/10.1016/j.jaap.2019.02.006, 2019.

1036 Stock, B. C., Jackson, A. L., Ward, E. J., Parnell, A. C., Phillips, D. L., and Semmens, B. X.: Analyzing
1037 mixing systems using a new generation of Bayesian tracer mixing models, PeerJ, 2018, 1–27,
1038 https://doi.org/10.7717/peerj.5096, 2018.

1039 Strong, D. J., Flecker, R., Valdes, P. J., Wilkinson, I. P., Rees, J. G., Zong, Y. Q., Lloyd, J. M., Garrett,
1040 E., and Pancost, R. D.: Organic matter distribution in the modern sediments of the Pearl River
1041 Estuary, Org Geochem, 49, 68–82, https://doi.org/10.1016/j.orggeochem.2012.04.011, 2012.

1042 Stronkhorst, J. and Van Hattum, B.: Contaminants of concern in Dutch marine harbor sediments, Arch
1043 Environ Contam Toxicol, 45, 306–316, https://doi.org/10.1007/s00244-003-0191-5, 2003.

1044 Szulc, W., Rutkowska, B., Gawroński, S., and Wszelaczyńska, E.: Possibilities of using organic waste
1045 after biological and physical processing—an overview, Processes, 9,
1046 https://doi.org/10.3390/pr9091501, 2021.

1047 Thornton, S. F. and McManus, J.: Application of organic carbon and nitrogen stable isotope and C/N
1048 ratios as source indicators of organic matter provenance in estuarine systems: Evidence from the tay
1049 estuary, Scotland, Estuar Coast Shelf Sci, 38, 219–233, https://doi.org/10.1006/ecss.1994.1015,
1050 1994.

1051 Tumuluru, J. S., Hess, J. R., Boardman, R. D., Wright, C. T., and Westover, T. L.: Formulation,
1052 pretreatment, and densification options to improve biomass specifications for Co-firing high
1053 percentages with coal, Industrial Biotechnology, 8, 113–132, https://doi.org/10.1089/ind.2012.0004,
1054 2012.

1055 van de Velde, S., van Lancker, V., Hidalgo-Martinez, S., Berelson, W. M., and Meysman, F. J. R.:
1056 Anthropogenic disturbance keeps the coastal seafloor biogeochemistry in a transient state, Sci Rep,
1057 8, 1–10, https://doi.org/10.1038/s41598-018-23925-y, 2018.

1058 Wakeham, S. G. and Canuel, E. A.: Degradation and preservation of organic matter in marine
1059 sediments, Handbook of Environmental Chemistry, Volume 2: Reactions and Processes, 2 N, 295–
1060 321, https://doi.org/10.1007/698_2_009, 2006.

1061 Wiesner, M. G., Haake, B., and Wirth, H.: Organic facies of surface sediments in the North Sea, Org
1062 Geochem, 15, 419–432, https://doi.org/10.1016/0146-6380(90)90169-Z, 1990.

1063 Wu, D., Deng, L., Liu, Y., Xi, D., Zou, H., Wang, R., Sha, Z., Pan, Y., Hou, L., and Liu, M.:
1064 Comparisons of the effects of different drying methods on soil nitrogen fractions: Insights into
1065 emissions of reactive nitrogen gases (HONO and NO), Atmospheric and Oceanic Science Letters, 13,
1066 224–231, https://doi.org/10.1080/16742834.2020.1733388, 2020.

1067 Yamamoto, S., Alcauskas, J. B., and Crozier, T. E.: Solubility of Methane in Distilled Water and
1068 Seawater, J Chem Eng Data, 21, 78–80, https://doi.org/10.1021/je60068a029, 1976.

1069 Zander, F., Heimovaara, T., and Gebert, J.: Spatial variability of organic matter degradability in tidal
1070 Elbe sediments, J Soils Sediments, 20, 2573–2587, https://doi.org/10.1007/s11368-020-02569-4,
1071 2020.

1072 Zander, F., Groengroeft, A., Eschenbach, A., Heimovaara, T. J., and Gebert, J.: Organic matter pools
1073 in sediments of the tidal Elbe river, Limnologica, 96, 125997,
1074 https://doi.org/10.1016/j.limno.2022.125997, 2022.

1075
1076
1077
1078
1079
1080
1081